The parent bodies of CR chondrites and their secondary history

Trygve Prestgard, Pierre Beck, Lydie Bonal, Jolantha Eschrig, Jérôme Gattacceca, Corinne Sonzogni, Lisa Krämer Ruggiu

The parent bodies of CR chondrites and their secondary history

Trygve Prestgard[1*], Pierre Beck[1], Lydie Bonal[1], Jolantha Eschrig[1], Jérôme Gattacceca[2], Corinne Sonzogni[2], Lisa Krämer Ruggiu[3]

[1]Institut de Planétologie et d'Astrophysique de Grenoble, Université Grenoble Alpes, CNRS CNES, 38000 Grenoble (France)
[2]CNRS, Aix Marseille Univ, IRD, Coll France, INRA, CEREGE, Aix-en-Provence, France
[3]Analytical-, Environmental- and Geo-Chemistry, Vrije Universiteit Brussel, Brussels, Belgium

* Corresponding author: trygve-johan.prestgard@univ-grenoble-alpes.fr.

To be submitted to Meteoritics & Planetary Science

Abstract:

Renazzo-type (CR) chondrites are a relatively rare group of carbonaceous chondrites with the vast majority having escaped thermal alteration (e.g., Schrader et al., 2015). This means that CRs are composed of relatively unprocessed material, depending on the extent of aqueous alteration they have experienced. Hydration in CRs ranges from incipient alteration of matrix glass, up to nearly complete replacement of the rock by hydration products. The extent of secondary processes is often difficult to assess in these meteorites, due to their heterogeneity and diversity of alteration products. Yet, this is crucial in order to understand the extent of geological processing that occurred on the primary parent body. Additionally, the parent asteroids of CRs remain a mystery, mainly because terrestrial oxyhydroxide signatures dominate the reflectance spectra of CRs. In this work, we have conducted optical and IR reflectance and transmission spectra of 25 CR chondrites in order to *(i)* better evaluate the extent of aqueous alteration that occurred on the CR parent body, and *(ii)* find possible parent body candidates. Terrestrial oxyhydroxides were removed from twelve samples, as these tend to interfere with the optical-IR spectra of CRs. Our results suggest, among other, that *(i)* aqueous alteration in most of our CRs was limited to the matrix and *(ii)* most CRs may stem from a continuum of X-to-C complex asteroids, depending on their extent of aqueous alteration. More specifically, the end members being Xk/Xn-types and Cgh/Ch-types. This has strong implication in regards to what we can expect from the Psyche mission.

1. Introduction

Renazzo-type (or CR) chondrites are rare carbonaceous chondrites, making a group of less than two hundred members (including paired samples). The group's namesake, Renazzo, fell on Earth in 1824, and is the first CR to have been discovered. It took over 130 years before the second member, Al Rais (a "fall", too), would be found. McSween (1977, 1979a) noted that both Renazzo and Al Rais, despite their various textural similarities with the CV group, were distinct in their chemical composition (including oxygen (O-)isotopic content) and by the presence of significant matrix phyllosilicates. McSween (1979) became the first to label these meteorites as "CR chondrites". With the start of systematic surveys in deserts in the 1970s, the number of "Renazzo-like" chondrites surpassed twenty by the 1990s. This eventually led to their official recognition as a distinct chemical group (Weisberg et al., 1993). Additionally, with the increase of meteorite discoveries and their chemical analysis, CRs were eventually found to be part of a chemical "clan", along the much rarer CH (Allan Hills [ALH] 85085-like) and CB (Bencubbin-like) chondrite groups (Bischoff et al., 1993, Weisberg et al.

2001). The CRs may also share affinities with a couple of ungrouped chondrites, more specifically, Lewis Cliff (LEW) 85332 (C3-ung) and Miller Range (MIL) 090292 (C1-ung: Jilly-Rehak et al., 2018).

CR chondrites are chemically reduced meteorites, characterized by large chondrules (~0.7 mm in average), high metal content (commonly between 5 – 8 vol%), rare refractory inclusions, and generally contain a matrix abundance of 30 – 50 vol% that tends to be aqueously altered. Metal is often present as large millimetric-sized grains, and very commonly as "blebs" surrounding chondrules (Weisberg et al., 1993; Krot and Scott, 2013; Schrader et al., 2014; Abreu, 2016). Fe-Ni sulfides are often present, but mainly in the matrix. To date, only three CR falls are known: Renazzo, Al Rais and Kaidun. The latter two however are atypical members, due to their high matrix abundance (Schrader et al., 2014), and high abundance and diversity of xenolithic clasts, respectively (e.g. Zolensky and Ivanov, 2003).

In addition to their rarity, CR chondrites appear to have experienced a large range of parent body processes. In fact, although most CRs are recognized as petrographic type-2 chondrites (meaning partially hydrated: Van Schmus and Wood, 1967), two CRs were found to have experienced significant shock-induced thermal metamorphism (Grosvenor Mountains [GRO] 03116 and Graves Nunataks [GRA] 06100: Briani et al., 2013), while one (GRO 95577) has been completely hydrated (type-1: Weisberg and Huber., 2007), hence the only known CR1 chondrite. In this meteorite, metal "blebs" have been almost entirely altered into magnetite, while chondrules appear as phyllosilicate pseudomorphs (Weisberg and Huber., 2007). MIL 090292 was previously labelled a CR1, before being reclassified as a C1-ung with possible affinities to the CR group (Jilly-Rehak et al., 2018).

Despite the range of secondary processing, most CRs have experienced only mild aqueous alteration of their matrices (e.g. Harju et al., 2014; Le Guillou et al., 2015), and have largely escaped thermal metamorphism (Schrader et al., 2015; Davidson et al., 2019). The relatively pristine nature of most CRs is further shown by their enrichment in ^{15}N (Krot et al., 2002) and by the high abundance of presolar grains in various members (Floss and Stadermann., 2009; Leitner et al., 2012; Davidson et al., 2014a). The relatively unprocessed nature of most CRs makes them precious targets for the compositional study of early solar system material.

The lack of obvious long-term (radiogenic-induced) thermal metamorphism suggests that the CR parent body accreted significantly later than those of many other chondrite groups, by the time a significant portion of ^{26}Al had already converted into ^{26}Mg (a major source of thermal metamorphism in type ≥3 chondrites (Kunihiro et al., 2004, Schrader et al., 2017; Budde et al., 2018). Van Kooten et al. (2016) alternatively suggest that this could be

explained if ^{26}Al was unevenly distributed in the solar system, hence CR material being ^{26}Al being poor even with an early accretion. Another scenario could be that the CR parent body was small, and thus did not incorporate sufficiently large volume/surface ratio of ^{26}Al to significantly metamorphose its interior. Recently however, one CR3 (Northwest Africa [NWA] 12474: thermal history similar to 3.1 chondrites), as well as five controversial CR6s and CR7s (e.g. NWA 7531 and NWA 12455), have been listed in the Meteoritical Society database, perhaps challenging this idea (Ruzicka et al. 2015a,b; Gattacceca et al., 2020a,b). In the case of the latter, these have more recently been suggested as being primitive achondrites with affinities to carbonaceous chondrites, and thus are not CRs (Ma et al., 2022).

In addition to their possibly relatively late-accretion, it is thought that the CR parent body might have formed at greater heliocentric distances than most chondrite groups (Van Kooten et al., 2016), a region that would coincide with that of comets (Van Kooten et al., 2016). In fact, a possible cometary-like clast has been reported in the CR2 LaPaz Icefield (LAP) 02342, thought to have been captured during its formation (Nittler et al., 2019). Other than Kaidun, carbonaceous xenoliths have also been found in CR2s such as Elephant Moraine (EET) 96259, NWA 14250 and Shişr 033 (Linstrom and Satterwhite, 1998; Russell et al., 2004; Gattacceca et al., 2022).

Unfortunately, despite our current knowledge of CRs, identification of their parent bodies remains a mystery. One difficulty is the high metal content of CRs, which rapidly convert to oxyhydroxides with terrestrial weathering. Consequently, these terrestrially-formed oxyhydroxides overshadow their innate silicate signatures in their VNIR spectra (Cloutis et al., 2012).

In regards to secondary classification, Alexander et al. (2013) and previously Howard et al. (2015) attempted to evaluate the extent of aqueous alteration in CRs based on their bulk content in hydrogen and phyllosilicates, respectively. Harju et al. (2014) evaluated the extent of aqueous alteration based on mineralogical indicators, notably the preservation of chondrule mesostasis, as well as the corrosion of silicates and metal into phyllosilicates and magnetite. Additionally, Schrader et al. (2011) found that the bulk oxygen isotopic composition of CRs correlated with aqueous alteration. Le Guillou et al. (2015) showed that the relative abundance of amorphous silicates, phyllosilicates and their $Fe^{3+}/\sum Fe$ state could be used as tracers of aqueous alteration. Spectroscopy has also been used to gain information on the secondary history of CRs. Indeed, Cloutis et al. (2012) and Beck et al. (2014) studied spectral properties of bulk CR powders in the optical and IR, and found indicators that could be related their secondary mineralogy. Bonal et al. (2013) studied the IR spectra of matrix grains,

deducing that they were phyllosilicate-rich. Briani et al. (2013) followed the same technique and found that the matrices of GRA 06100 and GRO 03116 were partially dehydrated, consistent with some thermal process (as described by Abreu, 2011, and Abreu and Bullock, 2013).

However, as discussed by Abreu (2016), finding a reliable indicator that allows, without exception, to characterize the extent of aqueous alteration has been challenging, especially among primitive CR2s. This is notably apparent by inconsistent petrographic types between different studies. These inconsistencies also arise, most likely, as a result of the heterogeneous nature of CR chondrites, many of which are likely breccia (e.g. Weisberg et al., 1993). This is equally applied to the matrix alone, for which variability can be observed within a single thin section (e.g. Wasson and Rubin, 2009). As previously described, according to the scale by Van Schmus and Wood (1967), CRs are classified as being type-1 or 2, meaning completely or partially hydrated. One can alternatively (and more precisely) subdivide these categories on a scale ranging from 2.0 – 2.9 (e.g. Harju et al., 2014), with 2.0 being completely hydrated (equivalent to type-1 by Van Schmus and Wood, 1967), while 2.9 would only have experienced very mild aqueous alteration. Other works rely on the petrologic grading system by Alexander et al., (2013), which is based on a scale from 1.0 to 2.9. In all three cases, type 3.0 would refer to ideally pristine rocks having experienced minimal parent body processes. The definition of each of these subcategories, particularly in the case of CRs, is sometimes arbitrary and mainly dependent on the methods used.

In the present work, we analyzed the spectral properties of 25 CR chondrites, with the objective to *(i)* better describe the extent of secondary processes they experienced, and *(ii)* to determine possible parent body candidates, by measuring the spectra of EATG leached powders (in order to remove iron oxides from the samples).

2. Method

2.1 Samples

A total of 25 CR chondrites were analyzed in this study (Table 1). The selected samples were mainly Antarctic finds (provided by ANSMET), however we additionally included a few hot-desert "finds" (provided by CEREGE), all of which we classified ourselves (NWA 12474, NWA 13724, NWA 14499 and NWA 14700). We also included a "fall" (Renazzo), which was provided to us from the Museo di Storia Naturale (Bologna). The CR chondrites that we selected for this study, according to the literature, were reported to have experienced various extents of secondary processes (i.e. aqueous alteration and thermal metamorphism). For

example, QUE 99177, Meteorite Hills (MET) 00426 and MIL 090657 have often been referred to as highly primitive CRs (e.g. Abreu and Brearley, 2010; Davidson et al., 2014a, 2019). Buckley Island (BUC) 10933 is reported as possibly having experienced a lower extent of aqueous alteration than typical CR2s (Ruzicka et al., 2015b). Dominion Range (DOM) 10085 was observed to be significantly shocked (Ruzicka et al., 2017); GRA 06100, GRO 03116 and NWA 12474 are heated (Abreu and Bullock, 2013; Briani et al., 2013; Gattacceca et al., 2020b) while GRO 95577 has been described as close-to-completely hydrated (CR1: Weisberg and Huber., 2007). We also wanted to include more recently-classified samples, that have yet to be extensively analyzed (e.g. our hot-desert finds, as well as GRO 17060). Renazzo, the only fall in our study, was important to include, as it provides a reference for comparison with our CR finds (as it has suffered a much lower degree of terrestrial weathering). Note that one of our samples, NWA 14250 contained multi-millimetric sized xenolithic clasts that were manually removed before our analysis. Table 1 summarizes the samples included in this study and the analysis that were conducted, along with references in the case of spectra extracted from previous studies.

For comparison to CR chondrites, we additionally included spectra obtained on various other carbonaceous chondrite groups: DOM 08006 (Prestgard and Bonal, 2019), and unpublished spectra of Acfer 094, Aydar 003, Lewis Cliff (LEW) 85311, NWA 11588, Orgueil and Wisconsin Range (WIS) 91600.

2.2 Transmission Spectroscopy of Bulk Samples

The prepared pellets consisted of a combination of KBr (300 mg of commercial ultrapure KBr powder), combined with 1 mg (0.9 – 1.3 mg) of meteorite powder (with the exception of 0.5 mg in the case of LAP 04516 and MIL 090001). The meteorite powder was extracted from a source of at least ~20 mg of an assorted sub-millimetric powder (generally more than 30 mg were available), which had previously been ground manually in a mortar. Although we prioritized the use of raw untreated (unleached) meteorite powders, we occasionally resorted to EATG (Ethanolamine Thioglycolate + Thioglycolate acid) leached powder (Table 1, see section 2.6 for details regarding EATG leaching), in the case of scarcely available raw material. This is because we found no strong differences between the mid-infrared (MIR) spectra of leached and untreated powders were observed (Fig. A: supplementary material), hence making it possible to use them interchangeably. Minor variations can be attributed to slight mineralogical heterogeneities of the powders, rather than effects due to the EATG leaching process.

As described in Prestgard et al. (2021): IR spectra were measured with a Brucker V70v spectrometer at the Institut de Planétologie et d'Astrophysique de Grenoble (IPAG, France). Spectra were acquired at 2 cm^{-1} spectral resolution in the 5000–400 cm^{-1} range (except for NWA 13724) under a primary vacuum ($P=10^{-3}$ mbar) or under ambient conditions. Spectra measured by Beck (2012), and Beck and Garenne (2012) were measured under 300°C while those in this work were conducted at ambient temperature.

Representativity: the bulk powder abundance was variable depending on the samples. Although most powders (both raw and leached) contained between 30 - 50 mg at the time of our study, only EET 92042 and MAC 87320 (raw powders) were between 20 and 25 mg. Their initial sample mass was however higher. In contrast, more than 100 mg were available for GRA 06100, GRO 03116, MET 00426, while over 50 mg were available for Renazzo. To verify the bulk representativity of our samples, we conducted a second set of measurements: multiple KBr pellets were prepared and measured of the initial source powders of MAC 87320, Renazzo and QUE 94603 (~30 mg). Fortunately, we were later granted additional raw fragments, those being EET 92042-90 (~130mg), MIL090657-56 (~335 mg), PCA 91082-54 (~170 mg), MIL 090001-120 (~190 mg), LAP 04720-22 (~200 mg).

Unfortunately, during this second session, we encountered mild issues with the ball-mill, which affected the quality of the mixing between our meteorite samples and the KBr powders. To overcome this, multiple spectra were measured each time. Fortunately, despite this issue, we found that most of these new spectra broadly agreed with the initial measurements (Fig. B in the supplementary materials), generally just mild differences in the 10-µm phyllosilicate-like band, which may possibly be an effect of the mixing, if not a very mild effect of heterogeneity.

To further support the overall bulk representativity of our samples, we also observed that the measurements between the leached and raw powders also tend to agree (see supplementary materials: Fig. A and B), these often being powders from different specific split fragments. Given the comparability of spectra for a single meteorite, this suggests that our data is representative of the bulk meteorites, and that the problems with the ball-mill did not severely affect our results.

The only exception was PCA 91082 and MIL 090001, both which showed more obvious variations in their phyllosilicate-like signatures (particularly PCA 91082). For MIL 090001, it may be because that 0.5 mg (instead of 1mg) were used for the sample preparation of the first spectrum. For PCA 91082, the spectrum published in Beck et al. (2014) differs significantly from those obtained in this work. The four that we obtained are more comparable, two of

those likely being from the same powder as from the one published by Beck et al. (2014). However, we do note those two show slightly stronger phyllosilicate-like signatures than those from PCA 91082-54. There may hence be some mild long-range mineralogical heterogeneity in this meteorite. The subject of sample representativity is particularly important in CRs, considering their heterogenous nature (e.g. Weisberg, 1993), and one that we discuss in section 4.2.

Note that certain spectra (one of EET 92042, and one of Renazzo) showed unusually strong enstatite signatures at ~9.3 μm (Fig. B). We however believe this to be due to the issues related to the ball-mill (i.e. grain size). The entirety of replicate measurements is shown in the supplementary materials (Fig. B), although all those of MIL 090001-120 and PCA 91082-54 are also included in Figs. 1 and 2.

2.3 Transmission Spectroscopy of Matrix Fragments

In the case of matrix fragments, IR spectra were obtained using a BRUKER HYPERION 3000 infrared microscope (IPAG, France). As described in Prestgard et al. (2021): The IR beam was focused through a 15x objective and the typical size of the spot on the sample was 40x40 μm². Spectra were measured at 4 cm^{-1} spectral resolution with an MCT detector cooled with liquid nitrogen.

Particular care was devoted to sample preparation, which is a critical issue in IR microspectroscopy. Samples must be thin (<20 μm) and their surfaces flat enough to avoid saturation of absorption and scattering artifacts, respectively (e.g. Raynal et al., 2000). Small matrix fragments (20–50 μm) were selected under a binocular microscope according to their color and texture. The matrix fragments were crushed between two diamond windows, allowing access to the 4000–650 cm^{-1} spectral range. Once split from, each separate diamond window were loaded into an environmental cell, designed, and built at IPAG. This cell enables temperatures up to 300°C to be reached under primary or secondary dynamic vacuum (from 10^{-4} mbar down to 10^{-7} mbar). Optical access is permitted from both sides of the cell through ZnS windows thus enabling measurements in transmission. Samples were heated up to 250 or 300°C, if not measured under ambient temperature. To remove interferences and scattering effects, a spline baseline was subtracted from the raw data. We then normalized the spectra according to the intensity of the Si-O stretching band, on a scale from 0-to-1.

These spectra used in this work are from Bonal (2011a-e) and Prestgard et al. (2021), which are accessible via the SSHADE database database:

https://www.sshade.eu/data/laboratory/LAB_IPAG

Representativity: The matrices of CR chondrites are known to be particularly heterogenous at the scales we study in this work (e.g. Wasson and Rubin, 2009). Moreover, CRs present Dark Inclusions (DIs) which can be difficult to distinguish from the matrix at first glance (e.g. Weisberg et al., 1993). This includes the case of our work. Hence, this is important to consider when interpreting our results.

Considering the size of matrix fragments that we selected, we measured at least five matrix grains (GRA 95229) up to ≥20 fragments in the case of QUE 99177, LAP 04720 and EET 92042. Hence, we cover several tens to hundreds of microns. We also measured n= 14 matrix fragments of "leached" QUE 99177 powder to see is any obvious mineralogical changes could be observed spectroscopically as a result of the leaching process (Fig. C. in suppl), which does not appear to be the case (implying that both powders could be measured interchangeably, depending on sample availability). Although the 10-µm Si-O region was studied in all spectra, the 3-µm region was only studied in spectra having been measured at 250 – 300°C. This is important to mention as small variations in the 10-µm band have been observed with heating. However, these variations have little-to-no impact on our interpretations. Note also that particularly as mild saturation may also mildly impact some of the spectra (see section 3.2 and 4.2).

Note that chondritic phyllosilicates and hydrated amorphous phases tend to be difficult to distinguish in the IR (e.g. Beck et al., 2014). Furthermore, phyllosilicates in CRs tend to be associated with amorphous phases at scales below those of our detection (e.g. Abreu and Brearley, 2010; Le Guillou et al., 2015; Abreu, 2016). Hence, in this work, we refer to any such bands as "phyllosilicate-like" signatures, prior to any extensive analysis (i.e. section 4.2.). Note that the matrix spectra do not necessarily stem from the same powders (i.e. specific slices) used for bulk measurements (sections 2.3. and 2.4.), which is to be noted in case of large-scale heterogeneity within CRs. In particular, no matrix IR spectra in this work were measured from the EET 92042-90, MIL 090657-56, LAP 04720-22 and PCA 91082-54 fragments.

2.4 IR spectra of matrix fragments from ALBA

One of the spectra presented in this work was acquired using the Infrared Microscopy and Spectroscopy (MIRAS) beamline at the ALBA synchrotron, in Spain. The sample preparation was done at IPAG (following the protocol described in 2.3) and brought to ALBA for analysis. The analysis was done in a nearly-identical manner to that done at IPAG; using a Vertex v70 FTIR (Fourier Transform infrared) spectrometer and a Hyperion 3000 IR

microscope (see section 2.3 for more details). Other than the origin of the radiation (being synchrotron radiation, in this case), the differences from section 2.3 were the size of the spot used (13 x 13 µm) and the temperature chosen for vacuum chamber. The samples were heated to 90°C, rather than 250 -300°C, to avoid the decomposition of innate organic matter present in the samples. Here we present the data obtained on a LAP 02342 matrix fragment (see sections 3.3 and 4.2).

2.5 Reflectance Spectroscopy

The reflectance spectra of our samples were acquired with the SHADOWS spectrogonio-radiometer (IPAG, France: Potin et al., 2018). The method used is that described by Prestgard et al. (2021): (1) We manually prepared 30–50 mg of an unsorted powder of submillimeter particle size using a mortar. Contrary to various other works (e.g., Cloutis et al., 2012), we chose not to sieve the powder in order to better represent the grain size heterogeneity expected of asteroidal regolith and avoid potential phase segregation. This is particularly important considering that the reflectance of CCs appear to be particularly controlled by its components (Garenne et al., 2016). (2) The sample was placed in an environmental chamber (MIRAGE) under vacuum ($P<10^{-4}$ mbar) at 80°C. This was done in order to remove weakly bonded water molecules. The chamber was enclosed by a sapphire window, whose optical contribution was removed from the raw spectra thanks to an adapted algorithm. (3) we chose an incidence angle of i=0° and an emergence angle of e=30°. The spectral resolution used varied from 0.048 to 0.39 m (with a step of 0.02 µm). Note that the measurements were normalized to reference surfaces, more specifically by using a Spectralon™ (for wavelengths 0.4–2.1 µm) and an Infragold™ (2.1–4.2 μm).

In addition to the powders, we measured the spectrum of a raw "chip" of the Renazzo, prior to it being crushed for the remainder of our measurements. This was done in ambient conditions (and then we did not consider the 3-µm region). Among the various powders, 12 samples were EATG leached, following the protocol used by Krämer Ruggiu et al. (2021). These are often distinct from the raw powders.

For the 3-µm region, we normalized the absorption band using a linear continuum (as in Eschrig et al., 2020). However, in addition, we normalized all bands to the same band depth, more specifically to 1 (see supplementary material). This is to be able to compare the profile of this band without interference of band depth (which is strongly influenced by the reflectance of our samples). To numerically compare these profiles, we calculated the ratio between the normalized band depth at various different wavelengths (what we refer to as

"normalized reflectance ratios"). The spectral metrics and their associated values are summarized in Table 2 and 3. We demonstrate this process in the supplementary materials (Fig. D).

Note that, for a some of the untreated reflectance spectra, optical data at wavelengths below 0.6 µm could not be used (Fig. E). Also, the overall reflectance of the untreated spectrum of EET 92159 might by slightly underestimated due to mild issues with the spectral correction.

Representativity: 30 – 50 mg of leached powders were measured (i.e. what the reflectance holder could take), which themselves were extracted from larger parent powders. Bulk representativity of such-sized powders are discussed in 2.2.

2.6 Oxygen Isotopic analysis

As described in Prestgard et al. (2021): Measurement of oxygen isotopic compositions of a 1.5 mg aliquot of bulk powdered BUC 10933 (182 mg), DOM 10085 (141 mg), GRO 17060 (216 mg) and NWA 12474 (411 mg) were carried out at the Stable Isotopes Laboratory of CEREGE (Aix-en-Provence, France) using laser fluorination coupled with isotope ratio mass spectrometry (ir-MS) (see e.g., Alexandre et al., 2006; Suavet et al., 2010 for more details about the analytical procedure). The initial sample mass was sufficient to ensure that measured aliquot is representative of the bulk. The three oxygen isotopic compositions were measured with a dual-inlet mass spectrometer Thermo-Finnigan Delta Plus. The oxygen isotope results are expressed in ‰ versus the international reference standard V-SMOW: $\delta^{18}O = [(^{18}O/^{16}O)_{sample}/(^{18}O/^{16}O)_{V\text{-}SMOW}\text{-}1]\times1000$ and $\delta^{17}O = [(^{17}O/^{16}O)_{sample}/(^{17}O/^{16}O)_{V\text{-}SMOW}\text{-}1]\times1000$. The $\delta^{18}O$ and $\delta^{17}O$ values of the reference gas were calibrated with measurements of NBS28 standard ($\delta^{18}O$=9.60‰, (Gröning 2004). $\Delta^{17}O$ is computed as $\Delta^{17}O = \ln(1+\delta^{17}O) - \lambda \times \ln(1+\delta^{18}O)$ with λ=0.52. The $\delta^{17}O$ value of the NBS28 standard ($\delta^{17}O$ =5.026‰) was computed so as to give $\Delta^{17}O$=0‰. The measurements were corrected on a daily basis using a 1.5 mg quartz internal laboratory standard "Boulangé" (Alexandre et al. 2006; Suavet et al. 2010). The analytical uncertainties derived from long term repeated measurement (n= 59) of this internal laboratory standard are 0.076‰, 0.139‰, and 0.013‰ for $\delta^{17}O$, $\delta^{18}O$, and $\Delta^{17}O$, respectively.

3. Results

3.1.Transmission Spectra of Bulk Samples

As can be seen in Figs. 1 and 2 transmission spectral profiles of our bulk 25 CR chondrites vary strongly from sample to sample. They can be subdivided into three overall "spectral

groups": *(i)* those that display profiles that are mainly consistent with a combination of pyroxene and olivine (most of our samples: Fig. 1); *(ii)* those dominated by phyllosilicates-like signatures (Fig. 2), *(iii)* samples dominated by olivine signatures (also Fig. 2). GRO 17060 is unusual in displaying only enstatite signatures in its spectrum.

The first group (Fig. 1) predominantly consist of primitive samples, classified as CR2.7 and CR2.8 by Harju et al. (2014) and CR2.5-2.8 by Howard et al. (2015) (see Table 4), while Davidson et al. (2019) classify MIL 090657 is listed as CR2.7 (scale by Alexander et al., 2013). Although many have not been provided a petrographic grade in the literature. The exceptions to this rule are GRO 03116 (CR2-heated: Abreu, 2011; Briani et al., 2013) and LAP 04720 (CR2.4 by Harju et al. 2014), although we note that GRO 03116 has a slightly stronger olivine signatures than most CRs in Fig 1, while LAP 04720 does present a weak resolvable phyllosilicate-like signature at 9.9 μm. Similar resolvable phyllosilicate-like signatures may be present in various other samples in Fig. 1: MAC 87320, NWA 13724, NWA 14499, LAP 02342, with the latter being a CR2.8 according to Harju et al. (2014). Note that most spectra of PCA 91082, from this work, resemble those of primitive CRs, while a few show weak phyllosilicate-like signatures. However, that of Beck et al. (2014) shows very noticeable phyllosilicate-like bands at 10-μm (see next paragraph, Fig. 2 and the supplementary materials).

In Fig. 2, we present IR spectra of samples that deviates from the typical enstatite-plus-olivine signature. Among them are CRs that display noticeable phyllosilicate-like signatures (at ~10.0 μm, ~15 μm and ~23 μm). Indeed, compared to the CRs in Fig. 1, Renazzo and MIL 090001 are labelled as CR2.4s by Harju et al, (2014), and PCA 91082 is a CR2.3 according to Alexander et al. (2013) and Howard et al. (2015). These latter observations of PCA 91082 are inconsistent with Schrader et al. (2015), who describe PCA 91082 as being comparably primitive to meteorites such as GRA 95229, LAP 02342 and QUE 99177, based on magnetite content in their chondrules and bulk O-isotopic composition. These observations are also not consistent with, Alexander et al. (2013), who found that Renazzo was comparably aqueously altered to the samples in Fig. 1, based on bulk H content. MIL 090001 appears to have the strongest signatures of phyllosilicates among these three meteorites.

We note that the spectrum of GRO 95577 is completely dominated by phyllosilicate-like signatures, consistent with its type-1 petrographic grade. Furthermore, as stated in Beck et al. (2014), the profile of GRO 95577 is particularly similar to that of CM1 chondrites. This is consistent with the serpentine-rich nature as first described during its initial classification (Linstrom & Satterwhite, 1997), but also in Weisberg and Hubert (2007).

The “olivine-rich” samples appear, at first glance, to be heated meteorites. Indeed, included are GRA 06100 (CR2-heated: Abreu and Bullock, 2013; Briani et al. 2013) and NWA 12474 (CR3). Although BUC 10933 and DOM 10085 have not been reported as heated CRs, the former has an anhydrous matrix (Cao et al., 2016), while the latter appears to be significantly shocked (Ruzicka et al., 2017). However, our oxygen isotopic measurements of BUC10933, DOM 10085 and NWA 12474 show that these are misclassified CV3 chondrites, which we will discuss in section 4.1. A detailed petrographic description of these meteorites can be found in the supplementary materials, which support these classifications. We also found GRO 17060 to be misclassified (section 4.1.)

Carbonate signatures do not tend to be very strong in our bulk IR CR chondrite spectra, but are detectable in many. They are best visible in GRO 17060 and the phyllosilicate-like rich samples.

3.2.Transmission Spectra of Matrix Fragments

With the exception of GRA 06100 and GRO 03116 (Briani et al., 2013), all spectra of CR2 matrix fragments measured in this work are characterized by strong, broad and relatively “round” 10-µm Si-O stretching bands (Fig. 3 and 4), consistent with phyllosilicate-like minerals, previously described by Bonal et al. (2013). The “squared” profile of GRO 95577 is likely the result of saturation. It may be possible that certain “round” IR profiles in MIL 090001 are also the result of mild saturation, considering the “sharp” phyllosilicate-like signatures in the spectra present in Fig. 2. There are more specific variations in the profile of these phyllosilicate-like bands, for example, certain have Lorentzian, gaussian, or “round”-profiles, and anything intermediate (their interpretations will be discussed in section 4.2).

Additionally, between 1800 – 700 cm^{-1}, most CR spectra also present lesser signatures due to Fe-poor olivine (~ 892 cm^{-1}) and/or carbonates (e.g. Fig. 3 and 4). In most CRs the intensity of these features varies strongly, especially within a single meteorite. Various examples are shown in Figs. 3.

Generally speaking, the matrix spectra of nearly all CR2s show some degree of olivine in their matrices, even if rare. Based on the average matrix spectra (Fig. 4), most matrices consist of primarily of phyllosilicate-like minerals and olivine (Fig. 4: gray). These have variable abundances of carbonate signatures, ranging from barely present (e.g. QUE 99177) to widespread and obvious (e.g. LAP 04720). Note that only the υ_3 (1500 – 1400 cm^{-1}) mode of carbonates is detectable in most matrix-average spectra of these meteorites, as the υ_2-mode (880 – 760 cm^{-1}), in-average, is overridden by olivine. Certain matrix spectra with particularly

strong carbonate signatures also show hints of the υ_4 mode at ~740 cm^{-1}. All of these meteorites have bulk IR spectra rich in olivine and enstatite (although PCA 91082 also has a bulk IR spectrum rich in phyllosilicate-like: Fig.2). Note that olivine signature in the matrix of LAP 02342 is, in-average, lower than that of CR2s of similar petrographic grades.

In contrast, GRA 95229 and MAC 87320 and NWA 14700 (Fig. 4: green) have matrices that in-appearance are particularly rich in carbonates compared to olivine, as both the υ_2 and υ_3 modes dominate the average matrix spectra. When looking at individual matrix spectra of these three meteorites, GRA 95229 and MAC 87320 (Fig. 3), show obvious olivine bands in various matrix fragments, compared to NWA 14700 where olivine is rare (Fig. 4). The two former have bulk IR spectra dominated by olivine and enstatite, while NWA 14700 is phyllosilicate-like rich (section 3.1 and Fig. 2.).

In comparison, Renazzo, MIL 090001 and GRO 95577 have IR matrix spectra dominated by phyllosilicate-like signatures, with the lack of strong carbonate and olivine signatures. They resemble the spectra of NWA 14700, but with less evidence of carbonates in the matrix fragments that we selected. This is interesting considering *(i)* traces of carbonates are visible in the bulk IR spectra of Renazzo and GRO95577, and *(ii)* have been reported to be quite abundant in GRO 95577 (5.7 vol% calcite) by PSD-XRD studies (Howard et al. 2015). Possible explanations to this discrepancy are discussed in section 4.2.

In regards to the 3-µm band, much like the Si-O stretching band, varies significantly depending on the meteorites, and within a single sample. Most notably is the peak wavelength of the band, symmetry and bandwidth (Fig. 3 and 4). Primitive CRs often display the largest diversity 3-µm profiles in their matrices. For example, in the case of LAP 02342, various matrix spectra display particularly broad 3-µm features (peaking around 3500 cm^{-1}), while others are more symmetric and peak at shorter wavelengths (larger wavenumbers). MIL 090001 and GRO 95577 appear to have more homogenous matrices, with profiles that, in average, are narrower, more asymmetric and peak at lower wavelengths than many LAP 02342 IR matrix spectra. Those of GRO 95577 appear to indicate more Mg-rich phyllosilicate-like minerals than MIL 090001.

Although, three Mg-rich phyllosilicate-like signatures were observed in matrix fragments of NWA 14700, they all happened to be saturated and hence could not be used to make Fig. 4. They are however present in the supplementary section (Fig. E).

We note, as mentioned in section 2.3., that our sample selection for matrix fragments cannot distinguish the fine-grained matrix from DIs, meaning that certain spectra are probably of DIs. We take this int account through our interpretations in section 4.2.

3.3 Reflectance Spectra of leached samples

Among all the selection of CR2 chondrites in this study, twelve meteorite powders have been leached and measured. In the VNIR region, compared to the untreated samples, the 0.9-µm bands, visual slopes have significantly decreased, and the drop-off is now at ~0.6 µm for all samples, rather than 0.7-0.8 µm (Fig 5). In contrast, the NIR slopes are overall redder. The overall VNIR reflectance was also observed to increase by 1% to ≥5% between leached and raw samples (the exception being MIL 090001, which decreased). We suspect that this general increase in reflectance and the reddening of the NIR slope is probably in part due to the loss of magnetite during the leaching process. Indeed, with the exception of moderately-severely hydrated CRs, all spectra of CR2 finds are dominated by signatures due to oxyhydroxides (consistent with Cloutis et al., 2012), probably of terrestrial origin. We provide a detailed description of the reflectance spectra of untreated powders in the supplementary material. This shows that the leaching process was successful at removing iron oxides and oxyhydroxides. Based on Fig. 6, we can subdivide these spectra into distinct groups:

- **Group 1:** QUE 99177, EET 92042, EET 92159 and GRA 95229: These meteorites display *(i)* strong and consistently red NIR slopes (likely due metal, and perhaps slightly to serpentine/chlorite), *(ii)* possible pyroxene bands at 0.9-µm and 1.8-µm and *(iii)* generally fainter 0.7-µm bands due to serpentine and/or chlorite. A faint band at 2.3-µm in GRA 95229 may be due to phyllosilicates. This group has the highest VNIR reflectance of all our samples (optical reflectance factor between ~0.12 and 0.18). The presence of pyroxene and phyllosilicates are consistent with our MIR transmission spectra. These meteorites are all listed as relatively primitive by Harju et al. (2014).
- **Group 2:** LAP 02342 and LAP 04516: The spectra of these meteorites are similar to the above group, with the exception of displaying relatively neutral NIR slopes. The optical reflectance remains comparable to the above group. Again, the presence of pyroxene and phyllosilicates are consistent with their MIR transmission spectra. The lack of a significant "metallic" VNIR red slope in these meteorites may suggest a lower bulk abundance of metal, in comparison. However, PSD-XRD measurements (Howard et al., 2015) did not indicate any significant difference in metal abundance between LAP 02342 and the previously-mentioned list.
- **Group 3:** Renazzo and MIL 090001: These spectra have a significantly lower VNIR reflectance than Groups 1 and 2. The spectrum of MIL 090001 strongly reflects serpentine (and/or chlorite), with a relatively weak 0.9-µm band (which is probably

comparably affected by both pyroxene and phyllosilicates). Renazzo's spectrum also reflects phyllosilicates, but displays a stronger 0.9-µm band, and an overall profile that still remains somewhat similar to Groups 1 and 2 (except a lack of a consistently red NIR slope). However, note that Renazzo was not treated in this study. Hence, as it is an old fall (1824), the spectrum (e.g. 0.9-µm band) may still be slightly contaminated by oxyhydroxides (Cloutis et al., 2012). Regardless, the presence of phyllosilicates is consistent with their MIR transmission spectra. The lack of a consistently red slope in these samples could indicate a lower bulk abundance of metal than Groups 1 and 2.

- **Group 4:** Contains only GRO 95577. The spectrum is purely dominated by phyllosilicate signatures, again consistent with the previous reflectance and transmission data obtained on this meteorite (see previous sections). The meteorite has the lowest VNIR reflectance of all our CRs (reflectance factor ~0.6).
- **Heated CRs**: GRO 03116 has a spectrum that best resembles LAP 02342, but lacks a clear presence of a 0.7-µm band. The VNIR reflectance of this meteorite is comparable to LAP 04516. GRA 06100, on the other hand, has shallow band at 1.05-µm due to olivine, and a red NIR slope, much like its spectrum of untreated powder (see section supplementary material). Its VNIR reflectance is comparable to MIL 090001 and Renazzo.

Similarly to the VNIR region, the 3-µm band profile is highly variable in regards to their profile (Fig. 6). Firstly, QUE 99177, LAP 02342 and LAP 04516 present broad bands that are centered at 3.06-µm. Seeing the expected lack of oxyhydroxides due to EATG leaching, these may be consistent with hydrated silicates of low crystallographic order. This would be consistent with the hydrated amorphous phases observed by Transmission Electron Microscopy (TEM) in CR2s (e.g. Abreu and Brearley, 2010; Le Guillou et al., 2015; Abreu, 2016). In the case of LAP 02342, this is particularly consistent with the high abundance of amorphous phases reported by Abreu (2016). However, LAP 04516, on the other hand, is considered particularly phyllosilicate-rich in the same study (see section 4.2).

Similarly to the previous samples, EET 92042, EET 92159, GRA 95229 and MIL 090001 (plus Renazzo) have broad 3-µm bands, but are centered at ~2.8-µm, most reminiscent of Fe-rich phyllosilicates. The broad nature of these bands may also be consistent with the contribution of additional amorphous phases, which have been reported in all these CR2 chondrites (Le Guillou et al., 2015; Abreu, 2016).

In the case of GRO 95577, its spectrum shows a particularly narrow 3-µm with a peak at 2.74 µm, indicating Mg-rich phyllosilicates-like minerals.

Lastly, in regards to the heated CRs, their spectra lack strong 3-µm bands, consistent with their partially dehydrated nature (Abreu, 2011; Abreu and Bullock, 2013; Briani et al., 2013).

Interestingly, when normalizing the 3-µm band profiles as described in the Method (section 2.5, and summarized in Tables 2 and 3), the Normalized 2.8/2.74 µm and 2.8/3.06-µm correlate well with the MIR spectra (Fig. 7). In fact, the samples can be subdivided into three groups: "primitive" CRs, "moderately hydrated" CR2s and CR1. These correlate well with the increasing phyllosilicate-like signatures in their bulk IR spectra (Fig. 1 and 2). This correlation is much less obvious in the case of untreated samples, due to the over-shadowing oxyhydroxide signatures (Fig. 7).

3.5 Bulk Oxygen isotopic analysis

We measured the bulk oxygen isotopic composition of three samples: BUC 10933, DOM 10085, GRO 17060 and NWA 12474. The obtained values are BUC 10933 ($\delta^{17}O$= -4.83; $\delta^{18}O$= -0.36), DOM 10085 ($\delta^{17}O$= -4,59; $\delta^{18}O$= -0,48), GRO 17060 ($\delta^{17}O$= 1.44; $\delta^{18}O$= 2.86) and NWA 12474 ($\delta^{17}O$= -4.34; $\delta^{18}O$= 0.34). The interpretation of this data will be provided in the following section.

4. Discussion

4.1 Reclassification of non-CR samples

As described in sections 3.1 and 3.5, BUC 10933, DOM 10085, NWA 12474 and GRO 17060 have peculiar spectral properties relative to most CRs. In the case of the first three, their olivine excess is apparent in the VNIR and MIR is similar to the heated CR GRA 06100 (Fig. 2), but also CO and CV chondrites (Beck et al., 2014, Eschrig et al., 2020, Prestgard et al., 2021). In contrast, we found that the spectrum of GRO 17060 we quite unique among all our samples (see previous sections and supplementary material). Consequently, we measured their bulk oxygen isotopic composition to verify whether or not they were misclassified (section 2.6).

Indeed, based on the values presented in section 3.5, we found that BUC 10933, DOM 10085 and NWA 12474 have bulk oxygen isotopic compositions consistent with CVs (Fig. 8), while that of GRO 17060 plots in a unique region along the Terrestrial Fractionation Line (TFL). Additionally, we analyzed sections of BUC 10933-34, DOM 10085-11 and NWA 12474 under a petrographic microscope, and found that their texture is most consistent with a

CV-reduced classification: *(i)* higher matrix abundance than most CRs (55 and 56 vol%, respectively, compared to 30 - 50 vol% for CRs: Krot and Scott, 2013), *(ii)* presence of abundant sulfides, including in chondrules, *(iii)* lack of metal blebs surrounding chondrules, with the exception of the obvious metal-sulfide rim(s) in BUC 10933, *(iv)* obvious CAIs in BUC 10933 and DOM 10085 (e.g. Fig. 9). The CV classification of BUC 10933 was already suspected by McAdam et al. (2015). We invite the reader to consult the supplementary data section for further details regarding the petrographic characterization of these samples.

Other misclassification between CV3-red and CR2 chondrites have occurred in the past (e.g. EET 96286, MIL 090001 and RBT 04133: Busemann et al., 2007; Keller et al. 2012; Davidson et al., 2014b) and are probably the result of the similar petrographic properties between both groups (as noted by McSween, 1979a). Note that Alexander and Bowden (2018) suggest that MIL 090001 may be related LEW 85332 (C3-ung), rather than CR2s, based on H, N and C bulk content and in their insoluble organic matter. Abreu (2016) also noted that MIL 090001 is petrographically distinct from other CRs, including its smaller average chondrule size than typical CRs, while Keller et al. (2012) found CAIs to be commonplace in MIL 090001, which is an atypical feature for CRs.

In the case of GRO 17060, seen its bulk oxygen isotopic composition, it is probably best associated with EH chondrites. This could be supported by *(i)* its enstatite-rich MIR spectrum; *(ii)* small average chondrule size compared to CRs (based on a preliminary analysis of a thin section); *(iii)* globally similar VNIR profiles to EHs (i.e. nearly featureless red slopes: RELAB database: https://pds-speclib.rsl.wustl.edu/search.aspx). Considering its hydrated nature (see supplementary materials) and the presence of carbonates, one should explore whether GRO 17060 may be the first "EH2" chondrite, or simply highly weathered. This is beyond the scope of this work.

4.2 Aqueous Alteration of unheated CR chondrites and effects of sample heterogeneity

In section 3.1, we observed that our transmission MIR spectra of bulk 25 CR chondrites could broadly be divided into three groups (section 3.1): *(i)* those rich in a combination of pyroxene and olivine, *(ii)* those with spectra dominated with phyllosilicates-like signatures and *(iii)* those presenting an olivine excess (only GRA 06100). PCA 91082 may be of *(i)* or *(ii)*. Generally, based on the petrographic grades provided in the literature (e.g. Harju et al., 2014; Howard et al., 2015: Table 2), the first group is mainly associated with primitive CRs, while *(ii)* and *(iii)* correspond to more hydrated (CR1 – 2.4) and heated CRs (GRA 06100),

respectively. We exclude BUC 10933, DOM 10085, GRO 17060 and NWA 12474 from this comparison, seen that they are not CR chondrites (see section 4.1).

Seen that the samples in Fig.1 do not show strong signatures due to phyllosilicate-like minerals (unlike the spectra of matrix fragments), it would mean that the bulk silicate content of CR2s is mostly anhydrous (i.e. olivine and enstatite). This is consistent with the high abundance of chondrules (50 – 60%: Krot and Scott, 2013), plus olivine being generally present in their matrices. This further means that any secondary processing that has predominantly affected the silicate mineralogy of the matrix may not be easily detectable in bulk IR spectra. It also implies that any hydrated silicates detected by reflectance (Fig. 6) should be confined to the matrix. Indeed, we find that the matrix mineralogy of CRs such as QUE 99177, GRA 95229 and GRO 03116 differ significantly, despite their comparable bulk IR spectra.

More specifically, based on section 3.2. and 3.3, the matrix of QUE 99177 should mainly consist of primary hydrated amorphous phases and probably olivine; GRA 95229 of Fe-rich phyllosilicates, carbonates, and olivine; GRO 03116 matrix is dehydrated and mainly consists of olivine. Heating in CRs (GRA 06100 and GRO 03116) will be discussed in the next section.

As described in the Method sections, we consider the spectra of bulk powders to be generally representative of the meteorites (although mild differences may present between spit slices in some, such as PCA 91082), although the IR spectra of matrix fragments may not necessarily be fully representative of the overall matrix content, and hence should be discussed with caution. Furthermore, certain "matrix" fragments may in fact be DIs, for which there is no way of verifying. Despite these limitations, these spectra do however provide insight into common minerals that are present in our CR matrices.

Based on the bulk IR and reflectance spectra of LAP 02342 and LAP 04516, these samples should be comparably altered to QUE 99177. The high abundance of amorphous phases in LAP 02342 is consistent with Abreu (2016), but not in the case of LAP 04516. In fact, Abreu (2016) described the amorphous phases in LAP 04516 as having been extensively replaced by phyllosilicates. This would suggest that *(i)* our LAP 04516 powder is less representative of the "bulk meteorite" than Abreu (2016), or *(ii)* other minerals are affecting the 3-µm band in our leached reflectance spectra in addition to hydrated silicates.

Regarding *(i)*, in section 2.1, all replicate IR spectra within a single meteorite were generally comparable (artefacts aside), although notable variations in phyllosilicate-like signatures might have been observed between split fragments within a couple meteorites.

Considering the differences observed between Abreu (2016) and this work, it would suggest that the extent aqueous alteration may have differed in both LAP 04516 fragments studied. The question is, how representative are our results compared to those of other studies (e.g. Abreu, 2016). Indeed, depending on the initial mass of our fragment (likely more than 50 mg), our sample may or may not be equally representative to studies such as Abreu (2016). Although, considering that the replicate IR spectra within a single sample powder (from tens to hundreds of milligrams) were nearly-always all comparable for our CRs (see supplementary materials, Fig. B), one could make the same assumption for our powder of LAP 04516, however no replicate spectra were available for this meteorite so this cannot be said with certainty.

Lastly, *(ii)* could possibly be explained by oxyhydroxides that have persisted in the leached powders of QUE 99177, LAP 02342 and LAP 04516, or rapidly formed after treating, contributing to the broad 3-µm band in their reflectance spectra. The third possibility is difficult to verify, but it would imply that the 3-µm reflectance profiles of QUE 99177 and LAP 02342 may also be "contaminated" by oxyhydroxides.

In the case of our matrix spectra of LAP 02342, we found three profiles similar to Mg-rich serpentine-smectite-like minerals in Orgueil. This means that *(i)* the matrix of this meteorite is heterogeneously altered at the scale of tens of microns (consistent with Wasson and Rubin, 2009 and Nittler et al., 2019). Evidence of smectite-like minerals are also found in other "primitive" CRs, including MET 00426 and QUE 99177 (e.g. Fig. 10). Additionally, Mg-rich serpentine-like is also possibly found in some matrix fragments of these CRs (e.g. one in MET 00426: Fig. 10). These results show that Mg-rich phyllosilicates (with different degrees of serpentine-like and smectite-like minerals) are present in the matrix (or in DIs) of our primitive CRs.

Matrix spectra showing Mg-rich phyllosilicates-like rarely show strong olivine signatures (Fig. 10), perhaps indicating that these fragments once contained Mg-rich olivine that was locally altered into Mg-rich phyllosilicates-like minerals. Alternatively, we speculate whether some of these matrix fragments may represent dark inclusions (DIs), as these tend to be hydrated (e.g. Abreu, 2016) and lack olivine. This is unfortunately impossible to verify.

We note that most of the IR matrix spectra that we collected for our primitive CR2s tend to display 10-µm band profiles similar to those that we collected from DOM 08006 (CO3.0), Acfer 094 (C2-ung) and LEW 85311 (CM2.7-an); all of which are also mildly altered objects. DOM 08006 contains a matrix rich in amorphous phases and olivine (e.g. Prestgard et al., 2021); Acfer 094 has a matrix rich in amorphous or "partially ordered" phases (Greshake,

1997, Ohtaki et al., 2021), while LEW85311 is rich in Fe-rich serpentine-like minerals (Lee et al., 2019). This is consistent with the amorphous phases and the nucleation of nanometric phyllosilicate crystals previously reported in CRs (e.g. Abreu and Brearley, 2010; Le Guillou et al, 2015). The presence of 0.7-µm bands in the reflectance spectra of all unheated EATG-leached CRs indicate the presence of Fe-rich serpentine and/or chlorite to some degree, even in those such as QUE 99177 and LAP 02342 that are particularly rich in amorphous phases compared to phyllosilicates. This indicates that the 0.7-µm band is particularly sensitive to serpentine and/or chlorite, despite their low degree of nucleation (i.e. short order).

Davidson et al. (2019) suggested MIL 090657 as possibly being less aqueously altered than other CRs studied based on its bulk δD and C/H content. Unfortunately, based on our available data (Fig. 1 and 4), we cannot set it apart from other primitive CR2s. EATG-leached spectra on MIL 090657 should be considered for future studies. The matrix fragments (n= 8) measured of this meteorite show amorphous or phyllosilicate-like phases, with lesser signatures due to olivine and carbonates, typical of most other of our CR2s.

Based on our interpretations so-far, knowing that the bulk IR spectra best reflects the chondrules, this would mean that phyllosilicate(-like)-dominated bulk IR spectra, such as those in Fig. 2, have experienced significant alteration of chondrule phenocrysts and matrix olivine (see section 3.3). This is consistent with the petrographic description provided by Harju et al. (2014) of Renazzo and MIL 090001. This is also consistent with NWA 14700 containing magnetite in silicate phenocrysts (Meteoritical society database: MB 111). Our IR spectral profiles of their matrices are probably most consistent with serpentine-like minerals, plus rare olivine, similar to those observed in CM2s (e.g. NWA 11588: Fig. 10). In fact, the bulk IR spectra of MIL 090001-120 shares resemblances with mildly altered CMs (e.g. MET 00633: Fig. 11), further supporting a strong spectral contribution of serpentine-like minerals. However, the 10-µm profile in MIL 090001 is slightly sharper than what we typically observe in CMs, which may possibly be a contribution due to saponite-like minerals. Again, traces of Fe-rich serpentine in and/or chlorite are present in the reflectance spectra (0.7-µm bands), as observed in all our EATG-leached powders (Fig. 6). Their presence in MIL 090001 is supported by Keller et al. (2012). Again, the profiles of the 3-µm bands of the matrix and reflectance spectra (Fig. 3, 6 and 7) suggest an average increase in Mg (relative to Fe) in phyllosilicate-like minerals compared to the primitive CRs. This can be explained by the liberation of Mg into the matrix as a result of chondrule corrosion, further supporting our interpretations of the bulk IR spectra.

Based on Fig. 2, the bulk phyllosilicate-like abundance of MIL 090001 is apparently higher than Renazzo, perhaps suggesting more advanced aqueous alteration. However, alternatively, this may be partially because MIL 090001 has a higher matrix abundance than Renazzo (based on Schrader et al., 2011 and Abreu, 2016). Hence, it is likely that our samples of Renazzo and MIL 090001 are comparably hydrated, which is possibly supported by their relatively similar matrix mineralogy (Fig. 4). However, as previously stated, the number of matrix fragments studied may not be representative of the entirety of their matrices. Moreover, the chondrule/matrix ratio may mildly vary at large scales from specific fragment-to-fragment, considering the differences reported between studies (e.g. Weisberg et al., 1993; Noguchi, 1995; Schrader et al., 2011; Abreu 2016).

As mentioned prior, LAP 04720 was listed as comparably altered to MIL 090001 according to Harju et al. (2014) as both were observed to have partially altered phenocryst. This phenocryst alteration was not observed by Abreu (2016) in LAP 04720 and MIL 090001. Interestingly, Abreu (2016) concluded that LAP 04720 was more altered than MIL 090001, yet MIL 090001 is the CR2 with the strongest bulk phyllosilicate-like signatures in our work (Fig. 2), while these are almost absent in the bulk IR spectrum of LAP 04720. Moreover, olivine is apparently widespread in nearly all our matrix spectra LAP 04720 (n= 20), unlike MIL 090001 which appears to have lost a lot of its matrix olivine based on the n=10 fragments selected (Fig. 3 and 4). Although MIL 090001 has a higher reported matrix abundance than LAP 04720 (25.8 area% versus 37.6 area%: Abreu, 2016), it is unlikely to explain their significant difference in phyllosilicate-like abundances alone.

Moreover, the strong phyllosilicate-like abundance (almost comparably to mildly altered CMs in the case of MIL 090001-120: Fig. 11), yet its matrix of only 37.6 area% (according to Abreu, 2016), we suspect that MIL 090001 did indeed suffer corrosion of its phenocryst, at least locally within our fragment MIL 090001-120, which agrees with the analysis by Harju et al. (2014). Although the chondrule/matrix ratio may mildly vary at large-scale within CRs, we can still support this argument as MET 00633 has a matrix abundance of 72% by point counting (Prestgard et al., 2022). Variations by a factor of two, between the matrix abundances measured by Abreu (2016) and in our samples is highly unlikely. This likely shows that MIL 090001 has experienced large-scale variations in regards to aqueous alteration, between the "bulk" samples used in study-to-study.

In contrast, our data of LAP 04720 points towards aqueous alteration having been limited to the matrix, which agrees with Abreu (2016). Moreover, considering that LAP 04720 and Renazzo likely have comparable matrix abundances (Schrader et al., 2011; Abreu, 2016), and

assuming our "bulk" powders are comparably representative for both meteorites, this means that our powders of LAP 04720 should be less aqueously altered than those of Renazzo. These results may again be further evidence of large-order mineralogical heterogeneity of CRs, particularly in regards to aqueous alteration. Indeed, Harju et al. (2014) might have sampled a relatively aqueously altered portion of this meteorite, unlike Abreu (2016) and ourselves.

Again, due to this possible large-scale heterogeneity within CRs, it begs the questions of whether the spectral variability (Fig. 1 and 2) observed between the PCA 91082 powder published by Beck et al. (2014) and those of PCA 91082-54 (this work) is a sampling bias (lower initial sample mass in the former, i.e. significant overrepresentation of the matrix compared to PCA 91082-54), or due to large-scale heterogeneity from fragment-to-fragment (the scale of ~100 mg or more), as possibly observed in LAP 04720 and MIL 090001 (above) between studies. Although this question may be impossible to answer, our spectra of PCA 91082-54 suggest that it is comparably primitive to most CRs in this study, which is consistent with Schrader et al. (2015). This same conclusion can also be applied to LAP 04516 (see above).

Consequently, the term "bulk representativity" is blurry in the case of CRs, as large scale mineralogical (probably beyond hundreds of milligrams) seem to exist in multiple CRs, as shown with LAP 04720 and MIL 090001 compared to Harju et al. (2014) and Abreu (2016). Hence, in this work, we must be particularly careful in our interpretations, considering that certain types measurements were not conducted of the same fragments (see section 2.3), and may thus not always be fully comparable. Although, on the flip-side, certain of our bulk IR measurements were conducted on multiple fragments (EET 92042, MIL 090001, LAP 04720, MIL 090657, PCA 91082), which provides additional useful information regarding large-scale heterogeneity. However, we cannot exclude the possibility that certain powders used in this study are less representative compared than that of other works (e.g. PCA 91082, see above).

Lastly, most silicates in GRO 95577 have been replaced by phyllosilicates, particularly Mg-rich serpentine-like minerals (Figs. 6 and 11) that vaguely resemble antigorite (by comparison with the standard mineral spectra presented in Fig. 1 by Beck et al., 2014). This is particularly consistent with its initial description by Linstrom & Satterwhite (1997), who described it to mainly consist of "isotropic to weakly birefringent serpentine". Note though that saponite is described as significantly present in this meteorite (e.g. Weisberg and Huber, 2007, Le Guillou et al., 2015). However, in GRO 95577 (and moderately altered CRs), these minerals

have probably mostly been overridden by serpentine-like signatures in the VNIR and MIR. This is unlike Orgueil (CI1) and WIS 91600 (C2-ung) which display noticeably distinct IR spectral profiles to CMs and CRs (Fig. 11), likely (in part) due to a stronger spectral contribution of smectite-like minerals. Indeed, CIs and WIS 91600 are also dominated by of smectite-serpentine-like phyllosilicates (e.g. Tomeoka, 1988; Tonui et al., 2014). However, we should note that phyllosilicates in WIS 91600 have been deformed through thermal metamorphism (Tonui et al., 2014), which may have affected its spectral properties, thus making a comparison with GRO 95577 difficult.

Our results suggest that serpentine-like phyllosilicates are a preferential aqueous alteration product in CRs, relative to CIs and WIS 91600. This progressive increase in Mg/Fe serpentine-like minerals in CRs with aqueous alteration is possibly reminiscent of that observed in CM chondrites (as first noted by McSween, 1979b), as observed spectrally by Beck et al. (2010). Furthermore, much like CMs, tochilinite has been reported in CR2s (Abreu, 2016), and is particularly associated with aqueous alteration in CMs (Jones and Brearley, 2006).

In section 3.4 we observed a decrease in the overall VNIR reflectance in the following order (leached and falls, excluding heated CRs): primitive (QUE 99177, EET 92159, EET 92042, GRA 95229, LAP 02342 and LAP 04516) > moderately hydrated (Renazzo, MIL 090001) > completely altered (GRO 95577). This can be interpreted as the decrease in metal with aqueous alteration (due to its transformation into magnetite, and oxyhydroxides (e.g. Abreu et al., 2016, 2020). This is further supported by the strong metal-like red slopes in the reflectance spectra of primitive CRs (with the exception of "Group 2" CRs LAP 02342 and LAP 04516), versus those that are more aqueously altered.

Lastly, we could potentially explain the lack of apparent carbonates in the matrix spectra due to sample preparation (a sampling bias). Indeed, we identify matrix fragments based on their porous and dark nature under a polarizing microscope (see section 2.3). With aqueous alteration (e.g. increased nucleation of carbonates), one could imagine that carbonate grains may conglomerate into larger structures, up to tens of microns, perhaps appearing as misleading "bright" sub-millimetric sized fragments under optical polarizing light. This is consistent with carbonates reported in GRO 95577, being tens of microns, or more, in diameter (Weisberg and Huber, 2007; Abreu, 2016). However, Abreu (2016) failed to detect significant calcite in MIL 090001. This shows that the carbonate signatures in our IR matrix spectra are most likely unrepresentative of what is truly present in the matrix (i.e. excludes

particularly carbonate-rich regions). Although, much like phyllosilicates, their heterogeneous presence is an indicator of an uneven distribution throughout their matrices.

To conclude, based solely on the powders that we studied, we tentatively suggest that the CRs in this study broadly underwent the following degree of aqueous alteration: (*i*) QUE 99177, LAP02342, LAP 04516 < (*ii*) EET 92042, EET 92159, GRA 95229 < (*iii*) Renazzo ≤ MIL 090001 << (*iv*) GRO 95577.

Our powders of LAP 04720, MIL 090657, QUE 94603, NWA 13724, NWA 14250 and NWA 14499 were possibly altered to a similar extent to (*i*) and (*ii*), based on IR spectra. NWA 14700 was probably similarly altered to (*iii*) due to its spectral similarities with Renazzo and MIL 090001. PCA 91082 could be either comparably altered to (*i*), *(ii)* and (*iii*), based on our limited data and uncertainties regarding sampling bias or large-scale mineralogical heterogeneities within these meteorites. As a result, providing petrological subtyping of CRs is particularly complex, and would probably require to study multiple split slices per meteorite.

4.3 Aqueous alteration in heated CRs: GRA 06100 and GRO 03116

Among our samples, two CR chondrites appear to have experienced short-term thermal metamorphism (e.g. Abreu, 2011; Abreu and Bullock, 2013; Briani et al., 2013; Schrader et al., 2015; Davidson et al., 2019): GRA 06100 and GRO 03116. As indicated by their reflection and IR spectra (including spectral data from Briani et al., 2013), preexisting hydrated silicates in both these meteorites have practically been dehydroxylated and were significantly recrystallized into olivine. Despite this, the bulk abundance of secondary olivine that resulted from this heating event(s) was significantly greater in GRA 06100 than in GRO 03116. A very weak 3-µm band is present in both their reflectance spectra, possibly indicating some low abundances of remaining water, newly formed (or remaining) oxyhydroxides and/or rare deformed phyllosilicates.

As discussed in the previous section, GRO 03116 has a bulk IR spectrum that is comparable to primitive CRs (those of which are listed as degrees *(i)* and *(ii)* in the previous section). This means that any secondary alteration that occurred in this meteorite was mild and probably did not significantly extend beyond the matrix. This implies that this meteorite was likely comparably hydrated to the primitive to the *(i)* and *(ii)* CRs prior to thermal metamorphism. This is supported by its reflectance spectrum, which shows obvious pyroxene signatures at 0.9 µm, typical of primitive CRs, probably indicating intact chondrules. According to Harju et al. (2014), GRO 03116 and GRA 95229 both showed similar incipient

pre-terrestrial magnetite in the matrix. Magnetite due to aqueous alteration was also described in GRO 03116 by Abreu (2011). Briani et al. (2013) considered GRO 03116 as being partially hydrated due to the presence of water in IR spectra of matrix fragments, although we wonder whether that detection may have been due to terrestrial oxyhydroxides, considering that this meteorite is quite weathered (e.g. Abreu, 2011). Interestingly, Howard et al. (2015) calculated 16.8 vol% of phyllosilicates in GRO 03116 by PSD-XRD, which is inconsistent with its dehydroxylated nature. The origin of this inconsistency is uncertain, considering that there is no spectroscopic evidence of intact phyllosilicates in our powders of these meteorites. A possibility may be that the sample studied by Howard et al. (2015) was less heated (and/or more aqueously altered) than ours, meaning that phyllosilicates persisted in their sample. This goes back to our discussion regarding the large-scale mineralogical heterogeneity of CRs (section 4.2).

Contrary to GRO 03116, thermal metamorphism in GRA 06100 would have resulted in a significantly greater abundance of secondary olivine, meaning that there was probably a higher abundance of hydrated silicates prior to heating. This implies that aqueous alteration must have extended beyond the matrix through chondrule corrosion, perhaps similarly to a moderately altered CR2s such as Renazzo. Chondrule corrosion is further supported by the lack of strong pyroxene signatures in the reflectance spectrum, unlike GRO 03116.

The more extensively hydrated nature of GRA 06100 is possibly supported by its lower abundance of metal than GRO 03116 (according to Howard et al., 2015), which may also be indicated by its lower reflectance than GRO 03116 (Fig. 6). Alternatively, Abreu and Bullock (2013) suggested that aqueous alteration in GRA 06100 was driven by the thermal event (possibly impact-driven), partially based on the petrography and composition of sulfides, oxides and metal.

According to Howard et al. (2015), GRO 03116 has a lower metal content than CRs such as QUE 99177 and GRA 95229. This may simply be due to the highly terrestrially weathered nature of the fragment studied by Howard et al. (2015), if their fragment is not more aqueously altered.

GRO 03116 and GRA 06100 were labelled as CR3.1 and CR3.6 by Abreu et al. (2020). However, seen that their thermal history is probably more analogous to short-term heating in CMs (Briani et al., 2013), rather than of long-term radiogenic origin (thermal history typical of type-3 chondrites), we believe that a designation similar to heated CMs by Tonui et al. (2014) and King et al. (2021) is appropriate for these meteorites: “CR2-Ts”, not CR3s.

4.4 The Parent Bodies of CR chondrites

By comparing our EATG leached reflectance spectra with those of mean asteroid spectral classes (by De Meo et al., 2009 and Binzel et al., 2019), we found that our CR chondrites do have spectroscopic similarities with a variety of asteroid spectral types, meaning that CRs could stem from a variety of different asteroids. This implies that certain asteroids of the following spectral types (and intermediates) may have coexisted within a common primary parent planetesimal. In the case of the unheated CRs, we noticed that the more primitive members (i.e. samples listed in Fig. 1) had stronger similarities with X-complex asteroids, notably the Xk-type (in the case of Group 1 CRs: QUE 99177, EET 92042, EET 92159, GRA 95229), and perhaps Xn-like (Group 2: LAP 02342, LAP 04516) (Fig. 13). CR2s did differ, however, by the additional presence of serpentine (or chlorite) absorption bands at 0.7-µm.

More hydrated CRs (e.g. MIL 090001 and GRO 95577), on the other hand, appear to better associate with C-complex asteroids, most notably of the Cgh and Ch-type. This is quite interesting, seen that *(i)* the Xk spectral type have already been associated with mesosiderites (Vernazza et al., 2016) and a CH3 chondrite (Krämer Ruggiu et al., 2021); *(ii)* Xn-type asteroids have not been affiliated with any known meteorite group; *(iii)* the Cgh spectral type have been mainly associated with CM(-like) chondrites (Vernazza et al., 2016; Krämer Ruggiu et al., 2021). Although, Beck et al. (2018) had already noted the Cgh-type spectrum of GRO 95577. It is thus interesting that certain CR2 chondrites may be analogous to this spectral class, too.

In the case of the heated CRs, the mildly-heated GRO 03116 has a stronger resemblance to the Xk or Xn spectral class, while that of GRA 06100 may appear more C or Cg-type-like. Moreover, the spectrum of the Renazzo chip is blue sloped (see section 3.4 and supplementary material), showing that the surface texture of parent bodies can further add to the diversity of parent body candidates.

A closer look at Fig. 13 suggests that our current collection of unheated CR chondrites stem from a continuum spanning the X-complex and C-complex asteroid types. X-complex asteroids would correspond to CR starting material (or mildly heated CR2s) and transform into Cgh/Ch profiles with increasing aqueous alteration.

We note however, that the overall reflectance of even the most hydrated CRs are significantly higher than what is commonly observed in CMs (optical reflectance factor between 0.05 and 0.1, compared to < 0.05 for most CMs), meaning that these types of CRs would perhaps stem from Cgh/Ch-type asteroids of higher albedo than those from which most CMs originate. However, by artificially crushing our leached powders (i.e. mimicking the

mechanical effects of space weathering), we found that their reflectance dropped significantly, even within the range of most CM chondrites. Hence, this may not exclude low albedo C-complex asteroids as the parents of hydrated CRs.

With the spectral-type and potential analogs in mind, we decided to look at the 3-µm bands of Xk, Xn, Cgh and Ch-type asteroids studied by Usui et al. (2019) via AKARI telescope data. Interestingly, in their work, several Xk and Xn-type appear to be hydrated. The peak absorption band of these asteroids were highly variable, ranging from ~3.1 µm in the case of (65) Cybele (Xk), down to 2.73 ±0.01 µm in the case of 56 (Melete). The 3-µm band position of Xk-type asteroids (55) Pandora is consistent with Xk-like CR2.6-CR2.8s, being located at 2.82±0.01 µm. In regards to Xn-types, (44) Nysa (the only Xn studied by Usui et al., 2019) shows signatures of hydration at ~3.08 ±0.01 µm, which is close to the peak 3-µm band position of LAP 02342 and LAP 04516.

Interestingly, asteroid (16) Psyche, the target of the Psyché mission, is a large Xk-type asteroid. Siltala and Granvik (2021) calculated that (16) Psyche has a bulk density of 3.88 $g.cm^{-1}$, which is lower than those of iron meteorite and somewhat comparable to mesosiderites (Siltala and Granvik, 2021). The authors suggest that this is in favor of the ferrovolcanism hypothesis by Johnson et al. (2020), in which the surface of (16) Psyche would be covered in a metal-rich layer that originated from the interior. This metal-rich layer would "hide" a more silicate-rich mantle of significantly lower density. Interestingly, by comparison with the density of chondrites made by Macke et al; (2011), the bulk density of (16) Psyche is most comparable to that of a CR2 chondrites (2.29 – 3.94 $g.cm^{-1}$) and a CH3 (Acfer 214: 3.77 $g.cm^{-1}$). Hence, alongside the spectral similarities, one could wonder if (16) Psyche consists of undifferentiated metal-rich (CH- or CR-like) carbonaceous chondrite material. This may be consistent with the presence of pyroxene signatures (0.9-µm absorption feature) on its surface (Sanchez et al., 2017). This could further support Xk-type asteroids being possible parents of primitive and reduced carbonaceous chondrites. However, Sanchez et al. (2017) suggest the silicate abundance to be quite low (only ~6%) based on experimental analogues and their spectra.

IR Observations of (16) Psyche have shown evidence of a 3-µm band attributable to hydrated silicates (Takir et al., 2017; Avdellidou et al., 2018). Some authors have considered the possibility of this hydrated material as being exogenic (e.g. Avdellidou et al., 2018), brought by carbonaceous chondrites. If (16) Psyche is composed of CR2 material, an endogenous origin is possible. On the other hand, the spectra of Usui et al. (2019) do not show a strong 3-µm band. In that case, if the surface of (16) Psyche is composed of CR2

material, it is possible that it has been mildly heated, and dehydrated, similarly to GRO 03116 (CR2-T). In the case of (16) Psyche however, one could imagine such heating mechanisms to be a product of space weathering, perhaps long-term micrometeorite bombardment and exposure to the solar wind.

Conclusion

Through oxygen isotopic analysis and petrographic observations, we conclude that BUC 10933 (CR2), DOM 10085 (CR2) and NWA 12474 (CR3) are misclassified reduced CV3 chondrites. GRO 17060, on the other hand, could be a hydrated EH chondrite candidate.

With increasing aqueous alteration, primary matrix phases (e.g. amorphous silicates and olivine) progressively transform into phyllosilicates. Carbonates also form and possibly nucleate into grains of tens of microns in diameter. Our reflectance spectra suggest that serpentine-like (and/or chlorite-like) minerals are already present in even the least altered CRs. Serpentine-like phases are particularly dominant in more altered CRs (e.g. MIL 090001 and GRO 95577). Much like for CMs, the relative Mg versus Fe content in phyllosilicate-like minerals is observed to increase with aqueous alteration in CRs, likely as a result of chondrule corrosion. Obvious evidence of smectite-like spectral profiles were only recognized in some matrix fragments of primitive CRs, although, our matrix measurements may not be fully representative of CR matrices and some may be DIs. Smectite-like spectral signatures are probably generally overshadowed by serpentine-like in CRs, particularly in more altered members. This suggests that serpentine-like minerals are a preferential alteration product in CRs, more so than in CIs and possibly WIS 91600 (C2-ung).

Based on our previous interpretations and observations alone, it is possible that our CR chondrites (at least the material that we studied) underwent the following order of aqueous alteration: QUE 99177, LAP 02342, LAP 04516 < EET 92042, EET 92159, GRA 95229 < Renazzo ≤ MIL 090001 << GRO 95577. Nine of the remaining CRs are possibly comparably primitive to QUE 99177 – GRA 95229, including LAP 04720. NWA 14700 is probably altered to a similar extent as Renazzo or MIL 090001. Although this order broadly agrees with the literature (particularly Harju et al., 2014), differences persist in regards to certain samples (e.g. LAP 04516, LAP 04720, MIL 090001 and PCA 91082). These differences may in some cases be induced by large-scale (what we would generally deem as “bulk representative”, i.e. ~100mg and more) heterogeneity in aqueous alteration or chondrule/matrix ratio (from fragment-to-fragment). If not, they could represent sampling biases due to less representativity in our powders than other studies, to the point of leading to

significant overrepresentation of chondrules or matrix (e.g. possibly PCA 91082). Regardless, it shows that spectroscopy can be powerful tools at studying aqueous alteration in CR chondrites.

The heated CRs GRO 03116 and GRA 06100 (at least our fragments) may have been comparably hydrated to QUE 99177 – GRA 95229 and Renazzo – MIL 090001, respectively, prior to a post-aqueous heating event. If these events are indeed post-aqueous, we suggest to label them as "CR2-T" chondrites, similarly to what is currently used for CMs (e.g. Tonui et al., 2014).

Finally, based on a comparison with mean asteroid spectra, we believe that primitive CR chondrites may stem from X-complex-like asteroids, notably Xk and Xn-like bodies. With increasing aqueous alteration, the increase in phyllosilicates such as serpentine cause the spectra to appear more Cgh-like, until eventually, purely resembling Cgh/Ch-type asteroids (i.e. CR1s). Hence, our current sampling of CRs may stem from a continuum of X-to-C-complex asteroids. The fact of that Xk asteroids may be associated with CH3 chondrites is indicative of this asteroid class being the parents of primitive and reduced carbonaceous chondrites. This has important implications on what we can expect from the Psyche mission's observations of Xk-type asteroid (16) Psyche.

Acknowledgments

We wish to thank ANSMET, CEREGE, and the Museo di Storia Naturale Università degli Studi di Firenze, for providing the meteorites that made this study possible. The SR-μFTIR experiment of LAP 02342 was performed at MIRAS beamline at ALBA Synchrotron with the collaboration of ALBA staff. We also wish to thank Dr. Eric Quirico, Dr. Rolando Rebois and Dr. Thai Van Phan for their help during this mission. We also wish to thank Edward Cloutis for the editorial handling, as well as the reviewers for their constructive and insightful comments. The mission was funded by the CNES. This work was funded by the European Research Council under the H2020 framework program/ERC grant agreement no. 771691(Solarys).

References

Abreu N. M. & Brearley A. J. 2010. Early solar system processes recorded in the matrices of two highly pristine CR3 carbonaceous chondrites, MET 00426 and QUE99177. *Geochimica et Cosmochimica Acta* 74(3):1146–1171.

Abreu N. M. 2011. Petrographic evidence of Shock Metamorphism in CR2 Chondrite GRO 03116. *Meteoritics & Planetary Science* 74(Suppl).

Abreu N. M., Bullock E. S. 2013. Opaque assemblages in CR2 Graves Nunataks (GRA) 06100 as indicators of shock-driven hydrothermal alteration in the CR chondrite parent body. *Meteoritics & Planetary Science* 48:2406–2429.

Abreu N. M. 2016. Why is it so difficult to classify Renazzo-type (CR) carbonaceous chondrites? – Implications from TEM observations of matrices for the sequences of aqueous alteration. *Geochimica et Cosmochimica Acta* 194:91–122

Abreu N. M., Aponte J. C., Cloutis E. A., Nguyen A. N. 2020. The Renazzo-like carbonaceous chondrites as resources to understand the origin, evolution, and exploration of the solar system. *Geochemistry* 80(4):125631

Alexander C. M. O'D, Howard K. T., Bowden R., Fogel M. L. 2013. The classification of CM and CR chondrites using bulk H, C and N abundances and isotopic compositions. *Geochemica et Cosmochemica Acta* 123:244-260.

Alexandre A., Basile-Doelsch I., Sonzogni C., Sylvestre F., Parron C., Meunier J.-D. et al. 2006. Oxygen isotope analyses of fine silica grains using laser-extraction technique: comparison with oxygen isotope data obtained from ion microprobe analyses and application to quartzite and silcrete cement investigation. *Geochimica et Cosmochimica Acta* 70(11):2827–2835.

Alexander C. M. O'D., Bowden R. 2018. Lewis Cliff (LEW) 85332 and Miller Range (MIL) 090001, a new Grouplet that is Distinct from the CR Chondrites?. *Meteoritics & Planetary Science* 81(Suppl).

Avdellidou C., Delbo M., Fienga A. 2018. Exogenous origin of hydration on asteroid (16) Psyche: the role of hydrated asteroid families. *Monthly Notices of the Royal Astronomical Society* 475(3):3419–3428

Battendier M., Bonal L., Quirico E., Beck P., Engrand C., Duprat T., Dartois E. 2018. Characterization of the organic matter and hydration state of Antarctic micrometeorites: A reservoir distinct from carbonaceous chondrites. *Icarus* 306:74–93.

Beck P., Quirico E., Montes-Hernandez G., Bonal L., Bollard J., Orthous-Daunay F.-R., Howard K. T., Schmitt B., Brissaud O., Deschamps F., Wunder B., Guillot S. 2010. Hydrous mineralogy of CM and CI chondrites from infrared spectroscopy and their relationship with low albedo asteroids. *Geochemica et Cosmochemica Acta* 74(16):4881–4892

Beck P. 2012: Mid-IR absorbance spectra of bulk CR chondrites in KBr pellets at ambient temperature, 150°C and 300°C. SSHADE/GhoSST (OSUG Data Center). Dataset/Spectral Data. https://doi.org/10.26302/SSHADE/EXPERIMENT_LB_20170725_001

Beck, P., Garenne, A., Quirico, E., Bonal, L., Montes-Hernandez, G., Moynier, F. et al. 2014. Transmission infrared spectra (2–25µm) of carbonaceous chondrites (CI, CM, CV–CK, CR, C2 ungrouped): mineralogy, water, and asteroidal processes. *Icarus* 229:263–277.

Beck P., Garenne A. 2012: Mid-IR absorbance spectra of bulk CM chondrites in KBr pellets at ambient temperature, 150°C and 300°C. SSHADE/GhoSST (OSUG Data Center). Dataset/Spectral Data. https://doi.org/10.26302/SSHADE/EXPERIMENT_LB_20170721_001

Beck, P., Maturilli, A., Garenne, A., Vernazza, P., Helbert, J.,Quirico, E. et al. 2018. What is controlling the reflectance spectra (0.35–150μm) of hydrated (and dehydrated) carbonaceous chondrites?. *Icarus* 313:124–138.

Binzel R. P., DeMeo F. E., Turtelboom E. V., et al. 2019. Compositional distributions and evolutionary processes for the near-Earth object population: Results from the MIT-Hawaii Near-Earth Object Spectroscopic Survey (MITHNEOS). *Icarus* 324: 41–76

Bischoff A., Palme H., Schultz L., Weber D., Weber H. R. Spettel B. 1993. Acfer 182 and paired samples, an iron-rich carbonaceous chondrite: Similarities with ALH85085 and relationship to CR chondrites. *Geochimica et Cosmochimica Acta* 57(11):2631–2648.

Briani G., Quirico E., Gounelle M., Paulhiac-Pison M., Montagnac G., Beck P., Orthous-Daunay F.-R., Bonal L., Jacquet J., Kearsley A., Russell S. S. 2013. Short duration thermal metamorphism in CR chondrites. *Geochimica et Cosmochimica Acta* 122(1):267–279

Bonal L. 2011a. Mid-IR absorbance spectra of EET92042 matrix grains under vacuum at different temperatures) under vacuum at 300°C. SSHADE/GhoSST (OSUG DataCenter). Dataset/Spectral Data. https://doi.org/10.26302/SSHADE/EXPERIMENT_LB_20170731_004.

Bonal L. 2011b. Raw, normalized and baseline-corrected of MIR transmission spectra of GRA95229 matrix grains pressed on diamonds under vacuum at ambient temperature and 300°C. SSHADE/GhoSST (OSUG Data Center). Dataset/Spectral Data. https://www.sshade.eu/data/experiment/EXPERIMENT_LB_20170731_003.

Bonal L. 2011c. Raw, normalized and baseline-corrected of MIR transmission spectra of MET00426 matrix grains pressed on diamonds under vacuum at ambient temperature and 300°C. SSHADE/GhoSST (OSUG Data Center). Dataset/Spectral Data. https://www.sshade.eu/data/experiment/EXPERIMENT_LB_20170731_001.

Bonal L. 2011d. MIR absorbance spectra of pressed QUE99177 matrix grains (CR Chondrite) under vacuum at different temperatures. SSHADE/GhoSST (OSUG DataCenter). Dataset/Spectral Data. https://www.sshade.eu/data/experiment/EXPERIMENT_LB_20170731_002.

Bonal L. 2011e. Mid-IR absorbance spectra of Renazzo matrix grains under vacuum at different temperatures. SSHADE/GhoSST (OSUG Data Center). Dataset/SpectralData. https://doi.org/10.26302/SSHADE/EXPERIMENT_LB_20170731_005.

Bonal L., Alexander C.M.O., Huss G.R., Nagashima K., Quirico, E. & Beck, P. 2013. Hydrogen isotopic composition of the water in CR chondrites. *Geochimica et Cosmochimica Acta* 106(1):111–133.

Busemann H., Alexander C. M.O'D, Nittler L. R. 2010. Characterization of insoluble organic matter in primitive meteorites by microRaman spectroscopy. *Meteoritics & planetary Science* 42(7–8):1387–1416.

Budde G., Kruijer T. S., Kleine T. 2018. Hf-W chronology of CR chondrites: Implications for the timescales of chondrule formation and the distribution of ^{26}Al in the solar nebula. *Geochimica et Cosmochimica* Acta 222:284-304.

Clayton R. N., Mayeda K. T., Rubin A. E. 1984. Oxygen isotopic compositions of enstatite chondrites and aubrites. *Journal of Geophysical Research Solid Earth* 89(1):245–249.

Cloutis E., Hudon P., Hiroi T., Gaffey M. & Mann, P. 2012. Spectral reflectance properties of carbonaceous chondrites—3: CR chondrites. Icarus 217(1):389–407.

Davidson J., Busemann H., Nittler L. R., Alexander C. M.O'D., Orthous-Daunay F.-R., Franchi I. A., Hoppe P. 2014a. Abundances of presolar silicon carbide grains in primitive meteorites determined by NanoSIMS. *Geochimica et Cosmochimica Acta* 139:248-266.

Davidson J., Schrader D. L., Alexander C.M.O'D, Lauretta D. S., Busemann H., et al. 2014b. Petrography, stable isotope compositions, microRaman spectroscopy, and presolar components of Roberts Massif 04133: A reduced CV3 carbonaceous chondrite. *Meteoritics & planetary Science* 49(12)2133–2151.

Davidson J., Schrader D. L., Alexander C. M.O'D., Nittler L. R., Bowden R. 2019. Re-examining thermal metamorphism of the Renazzo-like (CR) carbonaceous chondrites: Insights from pristine Miller Range 090657 and shock-heated Graves Nunataks 06100. *Geochimica et Cosmochimica Acta* 267:240-256.

DeMeo F. E., Binzel R. P., Slivan S. M., Bus S. J. 2009. An extension of the Bus asteroid taxonomy into the Near-Infrared. *Icarus* 202(1):160–180.

Eschrig, J., Bonal, L., Beck, P. & Prestgard, T.J. (2020) Spectral reflectance analysis of type 3 carbonaceouschondrites and search for their asteroidal parent bodies. *Icarus* 354:114034.

Floss C. and Stadermann F. J. 2009. High abundances of circumstellar and interstellar C-anomalous phases in the primitive CR3 chondrites QUE 99177 and MET 00426. *The Astrophysical Journal* 697:1242–1255.

Gattacceca J., Bonal L., Sonzogni C., Longerey J. 2020. CV chondrites: More than one parent body. *Earth and Planetary Science Letters* 547:116467.

Gattacceca J., McCubbin F. M., Bouvier A., Grossman J. N. 2020. The Meteoritical Bulletin, no. 108. *Meteoritics & Planetary Science* 55, 1146–115

Gattacceca J., McCubbin F. M., Bouvier A., Grossman J. N. 2020. The Meteoritical Bulletin, no. 107. *Meteoritics & Planetary Science* 55, 460–462

Gattacceca J., McCubbin F. M., Grossman J., Bouvier A., Chabot N. L., D'Orazio M., Goodrich C., Greshake A., Gross J., Komatsu M., Miao B., Schrader D. L. 2022. The Meteoritical Bulletin, No. 110. *Meteoritics & Planetary Science* 57, 2102–2105.

Greshake A. 1997. The primitive matrix components of the unique carbonaceous chondrite Acfer 094: A TEM study. *Geochimica et Cosmochimica Acta* 61(2)437 – 452

Harju E. R., Rubin A. E., Ahn I., Choi B.-G., Ziegler K., Wasson J. 2014. Progressive aqueous alteration of CR carbonaceous chondrites. *Geochimica et Cosmochimica Acta* 139:267–292.

Howard K. T., Alexander C.M.O'D., Schrader D. L., Dyl K. A. 2015. Classification of hydrous meteorites (CR, CM and C2 ungrouped) by phyllosilicate fraction: PSD-XRD modal mineralogy and planetesimal environments. *Geochemica et Cosmochemica Acta* 149:206–222.

Jilly-Rehak C. E., Huss G. R., Nagashima K., Schrader D. L. 2018. Low-temperature aqueous alteration on the CR chondrite parent body: Implications from in situ oxygen-isotope analyses. *Geochimica et Cosmochimica Acta* 222:230-252.

Johnson B. C., Sori M. M., Evans A. J. 2020. Ferrovolcanism on metal worlds and the origin of pallasites. *Nature Astronomy* 4:41–44.

Jones C. L., Brearley A. J. 2006. Experimental aqueous alteration of the Allende meteorite under oxidizing conditions: Constraints on asteroidal alteration. *Geochimica et Cosmochimica Acta* 70(4):1040-1058.

Kallemeyn G. W., Rubin A. E., Wasson J. T. 1994. The compositional classification of chondrites: VI. The CR carbonaceous chondrite group. Geochimica et Cosmochimica Acta 58(13):2873–2888.

Keller L. P., McKeegan K. D., Shard Z. D. (2012) The Oxygen Isotopic Composition of MIL 090001: A CR2 Chondrite with Abundant Refractory Inclusions (abstract #2065). 43rd *Lunar and Planetary Science Conference*. CD-ROM.

King A. J., Schofield P. F., Russell S. S. 2021. Thermal alteration of CM carbonaceous chondrites: mineralogical changes and metamorphic temperatures. *Geochimica et Cosmochimica Acta* 298:167–190.

Krot A. N., Meibom A., Weisberg M. K., Keil K. 2002. The CR chondrite clan: Implications for early solar system processes. *Meteoritics & planetary Science* 37:1451–1490.

Krämer Ruggiu L., Beck P., Gattacceca J., Eschrig J. 2021. Visible-infrared spectroscopy of ungrouped and rare meteorites brings further constraints on meteorite-asteroid connections. *Icarus* 362:114393

Kunihiro T., Rubin A. E., McKeegan K. D., Wasson J. T. 2004. Initial $^{26}Al/^{27}Al$ in carbonaceous-chondrite chondrules: too little ^{26}Al to melt asteroids. *Geochimica and Cosmochemica Acta* 68(13):2947–2957.

Lee M. R., Cohen B. E., King A. J., Greenwood R. C. 2019. The diversity of CM carbonaceous chondrite parent bodies explored using Lewis Cliff 85311. *Geochemica et Cosmochemica Acta* 264:224–244.

Le Guillou C., Changela H. G., Brearley A. J. 2015. Widespread oxidized and hydrated amorphous silicates in CR chondrites matrices: Implications for alteration conditions and H_2 degassing of asteroids. Earth and Planetary Science Letters 420:162–173

Leitner J., Vollmer C., Hoppe P., Zpifel, J. 2012. Characterization of Presolar Material in the CR Chondrite Northwest Africa 852. *The Astrophysical Journal* 745:38–54.

Lindstrom M. M., Satterwhite C.E. 1997. Antarctic Meteorite Newsletter 20(1).

Lindstrom M. M., Satterwhite C.E. 1998. Antarctic Meteorite Newsletter 21(2).

Marrocchi Y., Jacquet E., Neukampf J., Villeneuve J., Zolensky M. 2023. From whom Bells tolls: Reclassifying Bells among CR chondrites and implications for the formation conditions of CR parent bodies. *Meteoritics & Planetary Science* 42(2):195–206

Macke R. J., Consolmagno G. J., Britt D. T. 2011. Density, porosity, and magnetic susceptibility of carbonaceous chondrites. *Meteoritics & Planetary Science* 46(12)1842–1862.

Ma N., Neumann W., Neri A., Schwarz W. H., Ludwig T., Trielo M., Klahr H., Bouvier A. 2022. Early formation of primitive achondrites in an outer region of the protoplanetary disc. *Geochemical Perspective Letter* 23:33-37.

McSween, H. Y. Jr., Richardson, S. M. 1977. The composition of carbonaceous chondrite matrix. *Geochimica et Cosmochimica Acta* 41:1145–1161.

McSween, H. Y. Jr. 1979a. Are carbonaceous chondrites primitive or processed? A review. *Reviews of Geophysics and Space Physics* 17(5):1059–1078.

McSween H. Y.Jr. 1979b. Alteration in CM carbonaceous chondrites inferred from modal and chemical variations in matrix. *Geochimica and Cosmochimica Acta* 43:1761–1770.

Newton J., Franchi I. A., Phillinger C. T. 2000. The oxygen-isotopic record in enstatite meteorites. *Meteoritics & Planetary Science* 35(4)689–698.

Nittler L., Stroud R. M., Trigo-Rodríguez J. M., De Gregorio B.T., Alexander C. M.O'D., Davidson J., Moyano-Cambero C. E., Tanbakouei S. 2019. A cometary building block in a primitive asteroidal meteorite. *Nature Astronomy* 3:659–666.

Noguchi T. 1995. Petrology and mineralogy of the PCA 91082 chondrite and its comparison with the Yamato-793495 (CR) chondrite. Proc. *NIPR Symp. Antarctic Meteorites* 8:33–62.

Ohtaki K. K., Ishii H. A., Bradley J. P., Villalon K. L., Davis A. M., Stephan T., Bustillo K. C., Ciston J. 2021. Search for meteoritic GEMS I: Comparison of amorphous silicates in Paris and Acfer 094 chondrite matrices and in anhydrous chondritic interplanetary dust particles. *Geochimica et Cosmochimica Acta* 310(1):320 – 345

Potin S., Brissaud O., Beck P., Schmitt B., Magnard Y., Correia J.-J. et al. 2018. SHADOWS: a spectro-gonioradiometer for bidirectional reflectance studies of dark meteorites and terrestrial analogs: design, calibrations, and performances on challenging surfaces. *Applied Optics* 57(28), 8279–8296.

Potin S. & Beck P. 2019: NIR reflectance spectrum (i=0°, e=30°) of bulk CM, CR, CI and ungrouped chondrites under vacuum at room temperature before and after a heating cycle. SSHADE/GhoSST (OSUG Data Center). Dataset/Spectral Data. https://doi.org/10.26302/SSHADE/EXPERIMENT_LB_20191216_001

Prestgard T. & Bonal L. (2019) Raw MIR transmission spectra of matrix fragments of CO chondrites, pressed on diamonds under vacuum and at several temperatures. SSHADE/GhoSST (OSUG Data Center). Dataset/Spectral Data. doi: 10.26302/SSHADE/EXPERIMENT_LB_20201001_001

Prestgard T., Bonal L., Eschrig J., Gattacceca J., Sonzogni C., Beck P. 2021. Miller Range 07687 and its place within the CM-CO clan. *Meteoritics & Planetary Science* 56(9)1758–1783.

Prestgard T., Bonal L., Beck P. (2021): MIR absorbance spectra of pressed matrix grains from CR chondrites at variable conditions of temperature and pressure. SSHADE/GhoSST (OSUG Data Center). Dataset/Spectral Data. doi:10.26302/SSHADE/EXPERIMENT_LB_20221024_001

Prestgard T. J., Bonal L., Gattacceca J. Sonzogni C., Beck P. 2022. Exploring the connection between CM-CO clan chondrites through anomalous and misclassified members (abstract#6184). *Meteoritics & Planetary Science*, 85(Suppl.), 6184.pdf.

Raynal P. I., Quirico E., Borg J., Deboffle D., Dumas P., d'Hendecourt L. et al. 2000. Synchrotron infrared microscopy of micron-sized extraterrestrial grains. *Planetary and Space Science* 48:1329–1339.

Russell S. S., Folco L., Grady M. M., Zolensky M. E., Jones R., Righter K., Zipfel J., Grossman J. N. 2004. The Meteoritical Bulletin, No. 88, 2004 July. *Meteoritics & Planetary Science* 39(8). Supplement, A215–A272

Ruzicka A., Grossman J., Bouvier A., Herd C. D. K., and Agee C. B. 2015a. The Meteoritical Bulletin, No. 101. *Meteoritics & Planetary Science* 50:1661

Ruzicka A., Grossman J., Bouvier A., Herd C. D. K., and Agee C. B. 2015b. The Meteoritical Bulletin, No. 102. *Meteoritics & Planetary Science* 50:1662.

Ruzicka A., Grossman J., Bouvier A., Agee C. B. 2017. The Meteoritical Bulletin, No. 103. *Meteoritics & Planetary Science* 52:1014.

Siltala L. & Granvik M. 2021. Mass and Density of Asteroid (16) Psyche. *The Astrophysical Journal Letters* 909(1):14–19.

Sanchez J. A., Reddy V., Shepard M. K., Thomas C., Cloutis E. A., Takir D., Conrad A., Kiddell C., Applin D. 2017.Detection of Rotational Spectral Variations on the M-type asteroid (16) Psyche. *The Astronomical Journal* 153:29–37.

Schrader D. L., Franchi I. A., Connolly H. C. Jr., Greenwood R. C., Lauretta D. S., Gibson J. M. 2011. The formation and alteration of the Renazzo-like carbonaceous chondrites I: Implications of bulk-oxygen isotopic composition. *Geochimica et Cosmochimica Acta* 75(1):308–325.

Schrader D. L., Nagashima K., Krot A. N., Ogliore R. C., Hellebrand E. 2014. Variations in the O-isotope composition of gas during the formation of chondrules from the CR chondrites. *Geochimica et Comsochemica Acta* 132:50–74.

Schrader D. L., Connolly H. C. Jr., Lauretta D. S., Zega T. J., Davidson J., Domanik K. J. 2015. The formation and alteration of the Renazzo-like carbonaceous chondrites III: Toward understanding the genesis of ferromagnesian chondrules. *Meteoritics & Planetary Science* 50:15-50

Schrader D. L., Nagashima K., Krot A. N., Ogliore R. C., Yin Q.-Z., Amelin Y., Stirling C. H., Kaltenbach A. 2017. Distribution of 26Al in the CR chondrite chondrule-forming region of the protoplanetary disk. *Geochimica et Cosmochimica Acta* 201:275-302.

Scott E. R. D. and Krot A. N. 2014. Chondrites and their components. In Treatise on Geochemistry (2nd ed.), edited by Turekian H. D. H. K. Oxford: *Elsevier*. pp. 65–137.

Suavet C., Alexandre A., Franchi I. A., Gattacceca J., Sonzogni C., Greenwood, R.C. et al. 2010. Identification of the parent bodies of micrometeorites with high-precision oxygen isotope ratios. *EPSL*, 293, 313–320.

Takir D., Reddy V., Sanchez J. A., Shepard M. K., Emery J. P. 2017. Detection of Water and/or Hydroxyl on asteroid (16) Psyche. *The Astronomical Journal* 153:31–37.

Tomeoka K. & Busck P. R. 1988. Matrix mineralogy of the Orgueil CI carbonaceous chondrite. *Geochimica et Cosmochimica Acta* 52(1):1627–1640.

Tonui E., Zolensky M., Hiroi T., Nakamura T., Lipschutz M. E., Wang M.-S., Okudaira K. 2014. Petrographic, chemical and spectroscopic evidence for thermal metamorphism in carbonaceous chondrites I: CI and CM chondrites. *Geochimica et Cosmochimica Acta* 126:284–306.

Usui F., Hasegawa S., Ootsubo T., Onaka T. 2019. AKARI/IRC near-infrared asteroid spectroscopic survey: AcuA-spec. *Publications of the Astronomical Society of Japan* 71(1):1–41.

Van Kooten E. M. M., Weilandt D., Schiller M., Nagashima K., Thomen A., Larsen K. K., Olsen M. B., Nordlund Å., Krot A. N., Bizzarro M. 2016. Isotopic evidence for primordial molecular cloud material in metal-rich carbonaceous chondrites. *PNAS* 113(8):2011-2016.

Van Schmus W. R., Wood J. A. 1967. A chemical-petrologic classification for the chondritic meteorites. *Geochimica et Cosmochimica Acta* 31(5):747–754

Vernazza P., Marsset M., Beck P., Binzel R. P., Birlan M., Cloutis E. A., DeMeo F. E., Dumas C., Hiroi T. 2016. Compositional Homogeinity of CM Parent Bodies. *The Astronomical Journal* 152:54–64.

Yamanobe M., Nakamura T., Nakashima D. 2018. Oxygen isotope reservoirs in the outer asteroid belt inferred from oxygen isotope systematics of chondrule olivines and isolated forsterite and olivine grains in Tagish Lake-type carbonaceous chondrites, WIS 91600 and MET 00432. Polar *Science* 15:26–38. Weisberg M. K., Huber H. 2007. The GRO 95577 CR1 chondrite and hydration of the CR parent body. *Meteoritics & Planetary Science* 42(9):1495–1503

Wasson J. T., Rubin A. 2009. Composition of matrix in the CR chondrite LAP 02342. *Geochimica et Cosmochimica Acta* 73(5):1436–1460

Weisberg M. K., Prinz M., Clayton R. N., Mayeda T. K. 1993. The CR (Renazzo-type) carbonaceous chondrite group and its implications. Geochimica et Cosmochimica Acta 57(7):1567–1586.

Weisberg M. K., Prinz M., Clayton R. N., Mayeda T. K., Sugiura N., Zashu S., Ebihara M. 2001. A new metal-rich chondrite grouplet. *Meteoritics & Planetary Science* 36(3):401–418

Zolensky M., Ivanov, A. 2016. The Kaidun Microbreccia Meteorite: A Harvest from the Inner and Outer Asteroid Belt. *Geochemistry* 63(3):185–246

Tables and Figures

Table 1: Samples and spectral measurements conducted in this work

Sample	Transmission		Reflectance	
	Bulk	Matrix fragments	Untreated	EATG leached
BUC 10933	Yes	No	Yes	No
DOM 10085	Yes	No	Yes	No
EET 92042	Yes	Yes (n= 17)	Yes	Yes
EET 92159	Yes^	No	Yes	Yes

GRA 06100	Yes	No	Yes	Yes
GRA 95229	Yes	Yes (n= 5)	Yes	Yes
GRO 03116	Yes	No	Yes	Yes
GRO 95577	Yes	Yes* (n= 13)	Yes	Yes
NWA 14700	Yes	Yes (n= 10)	No	No
LAP 02342	Yes	Yes (n= 12)	No	Yes
LAP 04516	Yes**^	No	No	Yes
LAP 04720	Yes	Yes (n= 20)	Yes	No
MAC 87320	Yes	Yes (n= 9)	No	No
MET 00426	Yes	Yes (n= 11)	Yes	No
MIL 090001	Yes	Yes (n= 10)	Yes	Yes
MIL 090657	Yes	Yes" (n= 8)	Yes	No
NWA 12474	Yes	No	Yes	Yes
NWA 13724	Yes	Yes (n= 6)	Yes	No
NWA 14250	Yes	Yes (n= 9)	Yes	No
NWA 14499	Yes	Yes (n= 11)	Yes	No
PCA 91082	Yes	Yes (n= 6)	Yes	No
QUE 94603	Yes	Yes" (n= 6)	Yes	No
QUE 99177	Yes	Yes (n= 19)	Yes	Yes
Renazzo	Yes	Yes (n= 6)	Yes	No
GRO 17060	Yes	No	Yes	No

This table summarizes all the measurements conducted on the samples included in this study. Note that (*) refers to spectra that contained mild saturation of all the 10-µm Si-O silicate stretching bands, (**) refers to measurements conducted of leached powder, (^) 0.5 mg, rather than 1mg, of meteorite powder was used for the analysis, and (“) indicating that no matrix spectra were measured at 250 – 300°C. The table also shows the number (“n”) of matrix fragments analyzed in this study, not including one obtained using the ALBA/MIRAS beamline of LAP 02342. Various spectra used in this work (and included in this table) were available on the SSHADE database: Bonal (2011), Beck, (2012) and Potin (2019).

Table 2: Normalized 3-µm band parameters of untreated powder reflectance spectra

Designation	Location of band peak (µm)	Normalized reflectance ratio: 2.80/2.74 µm	Normalized reflectance ratio: 2.80/3.06 µm	Normalized reflectance ratio: 2.80/2.70 µm	Normalized reflectance ratio: 2.80/2.90 µm
QUE 99177	3.00	1.55	0.92	5.90	0.93
EET 92159	2.98	1.56	0.91	8.74	0.89
EET 92042	2.92	1.80	0.98	5.43	0.89
GRA 95229	2.96	2.01	0.91	7.04	0.85

MIL 090001	2.8	1.15	1.26	2.54	1.10
GRO 95577	2.75	0.92	1.41	1.62	1.17
GRO 03116	2.96	1.44	0.73	13.13	0.74
GRA 06100	2.9	1.47	0.76	15.82	0.62
PCA 91082	2.9	1.53	1.00	4.35	0.93
MIL 090657	2.9	1.78	0.93	6.18	0.82
MET 00426	2.88	1.45	0.97	3.65	0.90
Renazzo	2.78	1.08	1.22	3.47	0.98
NWA 14250	3.12	1.77	0.75	11.19	0.82
NWA 14499	2.98	1.42	0.99	2.85	0.93
NWA 13724	3.00	1.48	0.93	3.82	0.94
LAP 04720	2.94	2.01	0.90	14.19	0.83

Here we summarize the spectral metrics of the 3-µm band (of reflectance spectra) that we calculated for untreated (raw) powders. More specifically, these values refer to the "normalized" 3-µm bands (method described in section 2.5).

Table 3: Normalized 3-µm band parameters of leached powder reflectance spectra, and Renazzo.

Designation	Location of band peak (µm)	Normalized reflectance ratio: 2.80/2.74 µm	Normalized reflectance ratio: 2.80/3.06 µm	Normalized reflectance ratio: 2.80/2.70 µm	Normalized reflectance ratio: 2.80/2.90 µm
QUE 99177	3.06	1.80	0.94	4.80	0.98
EET 92159	2.82	1.63	1.07	4.75	1.02
EET 92042	2.8	1.49	1.20	3.10	1.10
GRA 95229	2.82	1.62	1.10	5.37	1.05
LAP 04516	2.90	1.66	0.94	4.81	0.94
LAP 02342	3.06	1.52	0.96	2.83	1.01
MIL 090001	2.78	1.11	1.18	2.12	1.09
GRO 95577	2.74	0.85	1.47	1.15	1.27
GRO 03116	3.06	1.69	0.71	2.05	0.79
GRA 06100	3.06	1.67	0.49	46.69	0.54
Renazzo	2.78	1.08	1.22	3.47	0.98

Here we summarize the spectral metrics of the 3-µm band (of reflectance spectra) that we calculated for EATG leached powders. More specifically, these values refer to the "normalized" 3-µm bands (method described in section 2.5).

Table 4: Petrographic grades of our samples and other works

Sample	Alexander 2013	Harju et al. (2014)	Howard et al. (2015)	Remarks
BUC 10933				*CV3 (Reduced)*
DOM 10085				*CV3 (Reduced)*
NWA 12474				*CV3 (Reduced)*

EET 92042	2.5	2.8		
EET 92159				Paired with EET 92042
GRA 06100		2.5	2.8	Heated CR2
GRA 95229	2.5	2.7	2.8	
GRO 03116		2.7	2.5	Heated CR2
GRO 95577	1.3	2.0	1.6	
NWA 14700				
LAP 02342	2.5	2.8	2.7	
LAP 04516	2.6	2.8		
LAP 04720		2.4		
MAC 87320				
MET 00426	2.6	2.8	2.6	
MIL 090001		2.4		
MIL 090657	*2.7**			
NWA 13724				
NWA 14250				
NWA 14499				
PCA 91082	2.3			
QUE 94603				
QUE 99177	2.4	2.8	2.8	
Renazzo	2.5	2.4		
GRO 17060				*EH(-like) Chondrite*

Summary of the various petrographic grades that have been attributed in the literature, plus additional remarks. We suggest to refer to GRA 06100 and GRO 03116 as "CR2-T" chondrites, as they experienced short-term thermal metamorphism, probably similar to many heated CMs (Briani et al. 2013). Three of the samples are confirmed to be CV3s: BUC 10933, DOM 10085 and NWA 12474 (see section 4.1). GRO 17060 may be hydrated meteorite with affinities to EH chondrites (these misclassified objects are written in italics). The asterisk (*) refers to values derived by Davidson et al. (2019) using the scale of Alexander et al. (2013). Note that the grading system used by Alexander et al. (2013) is not the same "scale" as those used in the other studies.

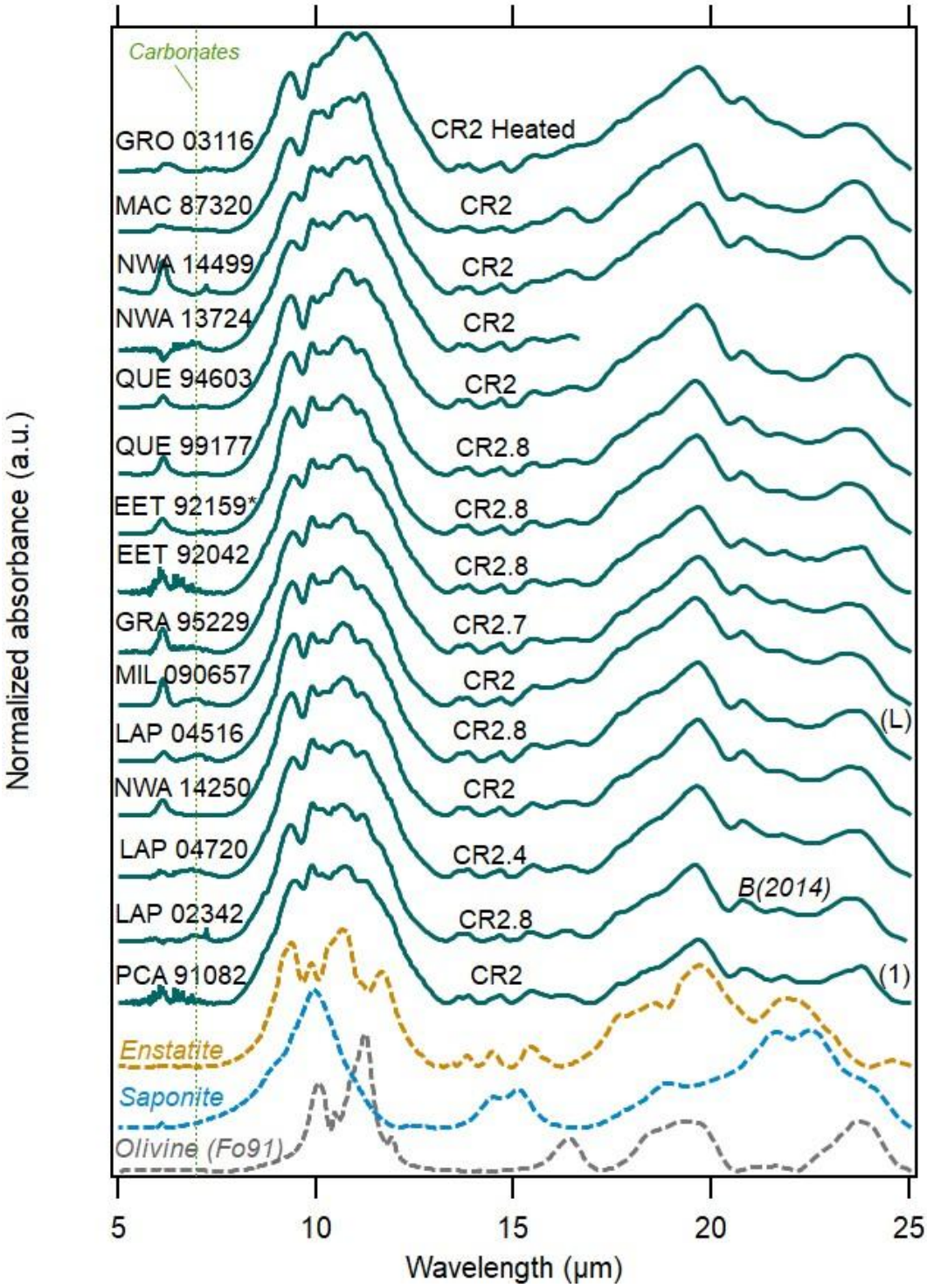

Fig. 1: MIR spectra of bulk CR material. More specifically, this graph plots those CR spectra that are dominated enstatite and olivine signatures. The green vertical line denotates carbonates. The spectra are normalized to the maximum intensity of the Si-O (10-μm) stretching band. (L) refers to powders that were EATG leached, while the numbers are added in the case of multiple IR spectra having been plotted. In this case, PCA 91082, which also has a spectrum that appears in Fig. 2. The asterisk refers to KBr pellets that were made using 0.5 mg of meteorite powder, rather than 1mg. The petrographic

grades used in this figure are those attributed by Harju et al. (2014). Offset has been added for the purpose clarity.

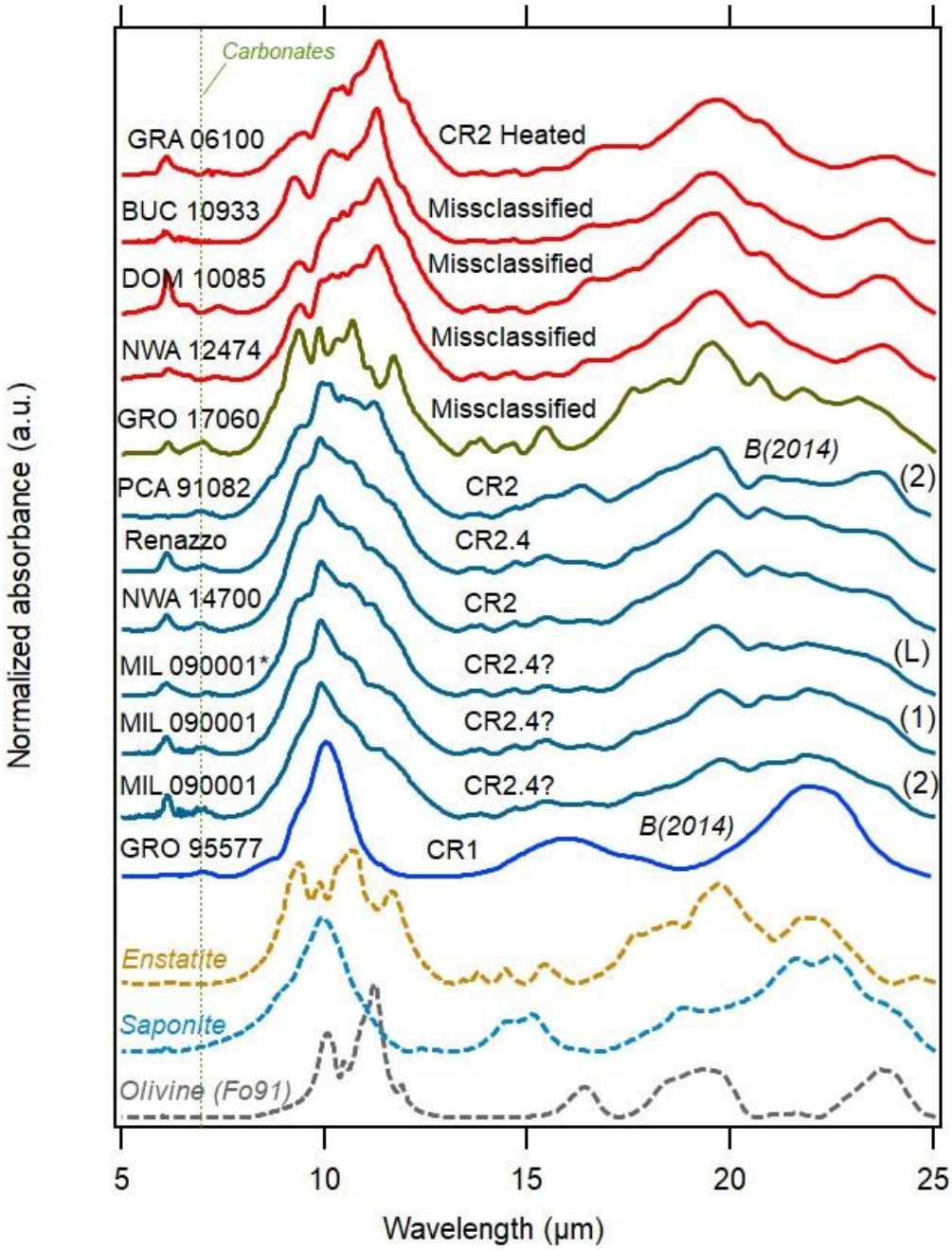

Fig. 2: MIR spectra of bulk CR material. More specifically, this graph plots those spectra that are dominated by olivine (red), phyllosilicates (blue), and purely-enstatite (brown: GRO 17060). The green vertical line denotates carbonates. The spectra are normalized to the maximum intensity of the Si-O (10-μm) stretching band. (L) refers to powders that were EATG leached, while the numbers are added in the case of multiple IR spectra having been plotted. In this case, MIL 090001 and PCA 91082. The latter also has a spectrum that appears in Fig. 1. The asterisk refers to KBr pellets that were made using 0.5 mg of meteorite powder, rather than 1mg. Note that four samples are misclassified, based on our work, while MIL 090001 has been suspected of not being a CR by other

authors (see section 4.1.). The petrographic grades used in this figure are those attributed by Harju et al. (2014), Weisberg and Huber (2007), and based on Briani et al. (2013). Offset has been added for the purpose clarity.

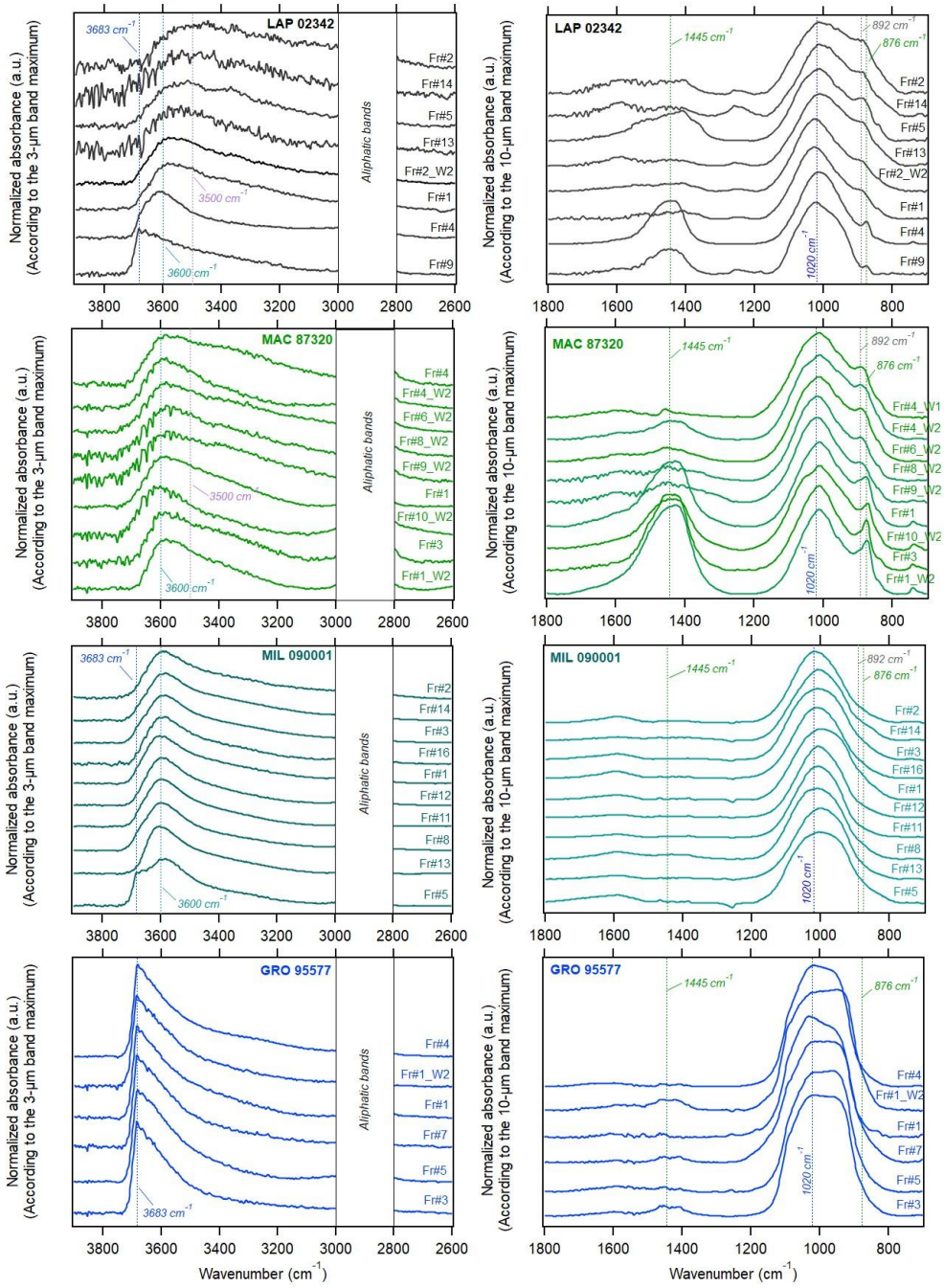

Fig. 3: Examples of IR spectra taken of various CR matrix fragments meteorites having undergone different degrees of aqueous alteration. Those of LAP 02342 are particularly heterogenous, which is also the case of several other mildly altered CRs. The contrary can be said about MIL 090001 and GRO95577, which are significantly more aqueously altered. Note that each set of spectra have been normalized differently. Those at 3-µm are the average of individual spectra normalized to the peak of the 3-µm band, while those at 10-µm the average of individual spectra normalized according to the peak at 10-µm. All spectra in this plot were taken at 250°C. Regarding the vertical lines, blue (1020

cm^{-1}) correspond to phyllosilicate-like minerals; green (1445 and 876 cm^{-1}) correspond to carbonates and gray to olivine (892 cm^{-1}). Offset has been added for the purpose clarity.

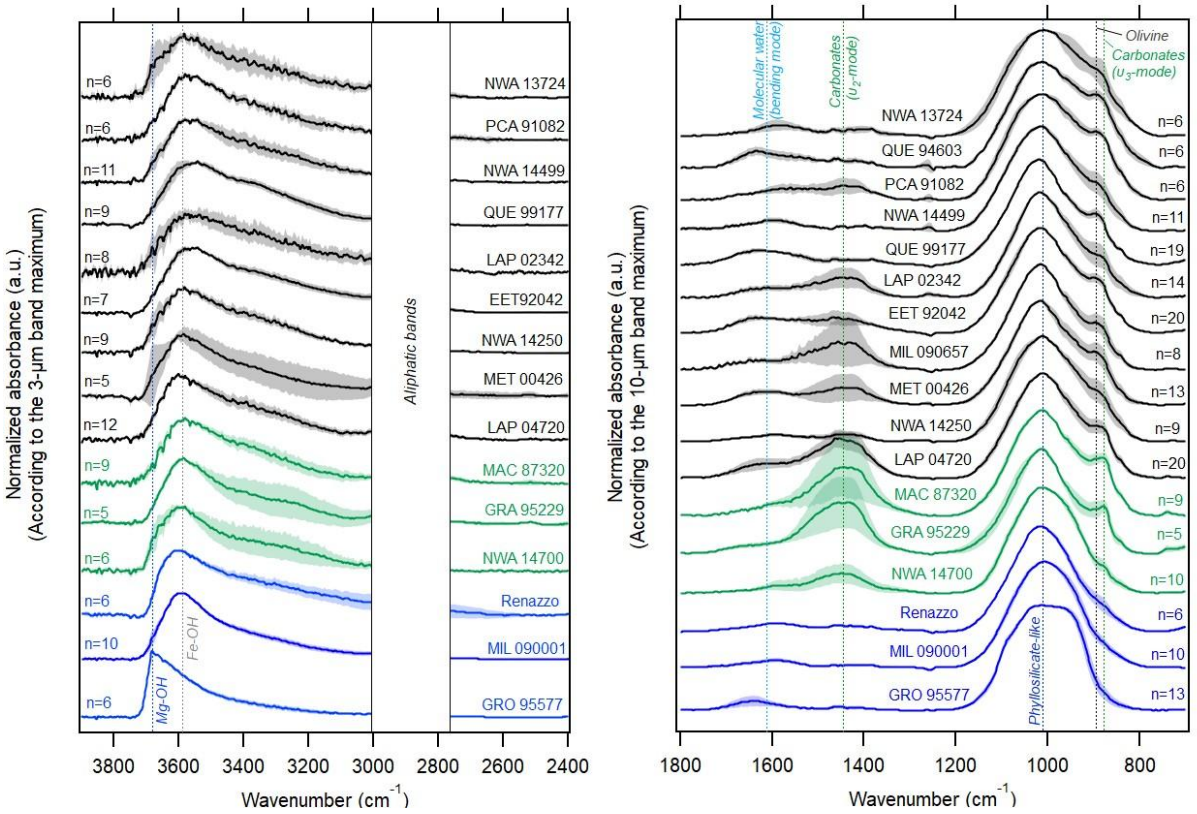

Fig. 4: Average of all successful matrix fragment spectra for each meteorite. In black the spectra showing strong olivine signatures; in green those with strong carbonate signatures; in blue those predominantly containing phyllosilicate-like signatures. The number of individual spectra used for the averages ("n") differs between both the 3-µm and 10-µm as *(i)* only spectra taken between 250 – 300°C could be used to study the 3-µm region, while the 10-µm band also includes all the spectra taken at ambient temperature; *(ii)* some spectra were of lower quality in the 3-µm region compared to the 10-µm region, or vice-versa. Moreover, note that each set of spectra have been normalized differently. Those at 3-µm are the average of individual spectra normalized to the peak of the 3-µm band, while those at 10-µm the average of individual spectra normalized according to the peak at 10-µm. Offset has been added for the purpose clarity.

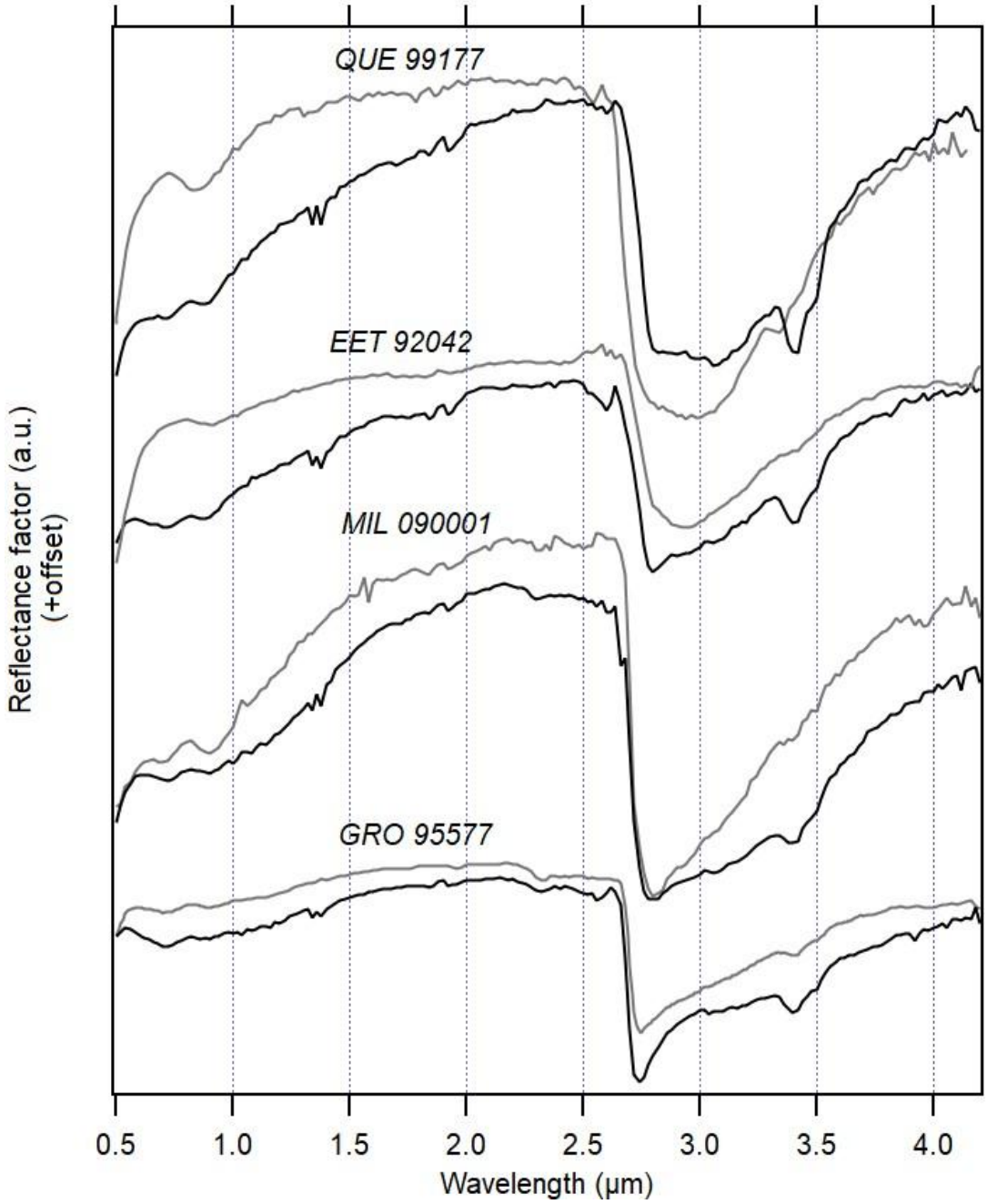

Fig. 5: Comparison between reflectance spectra of raw untreated powder (gray) compared to that of EATG leached powder (black). Notice the decrease in visual slope, 0.9-μm band, and a generally sharper 3-μm band with the exception of MIL 090001). Offset has been added for the purpose of clarity.

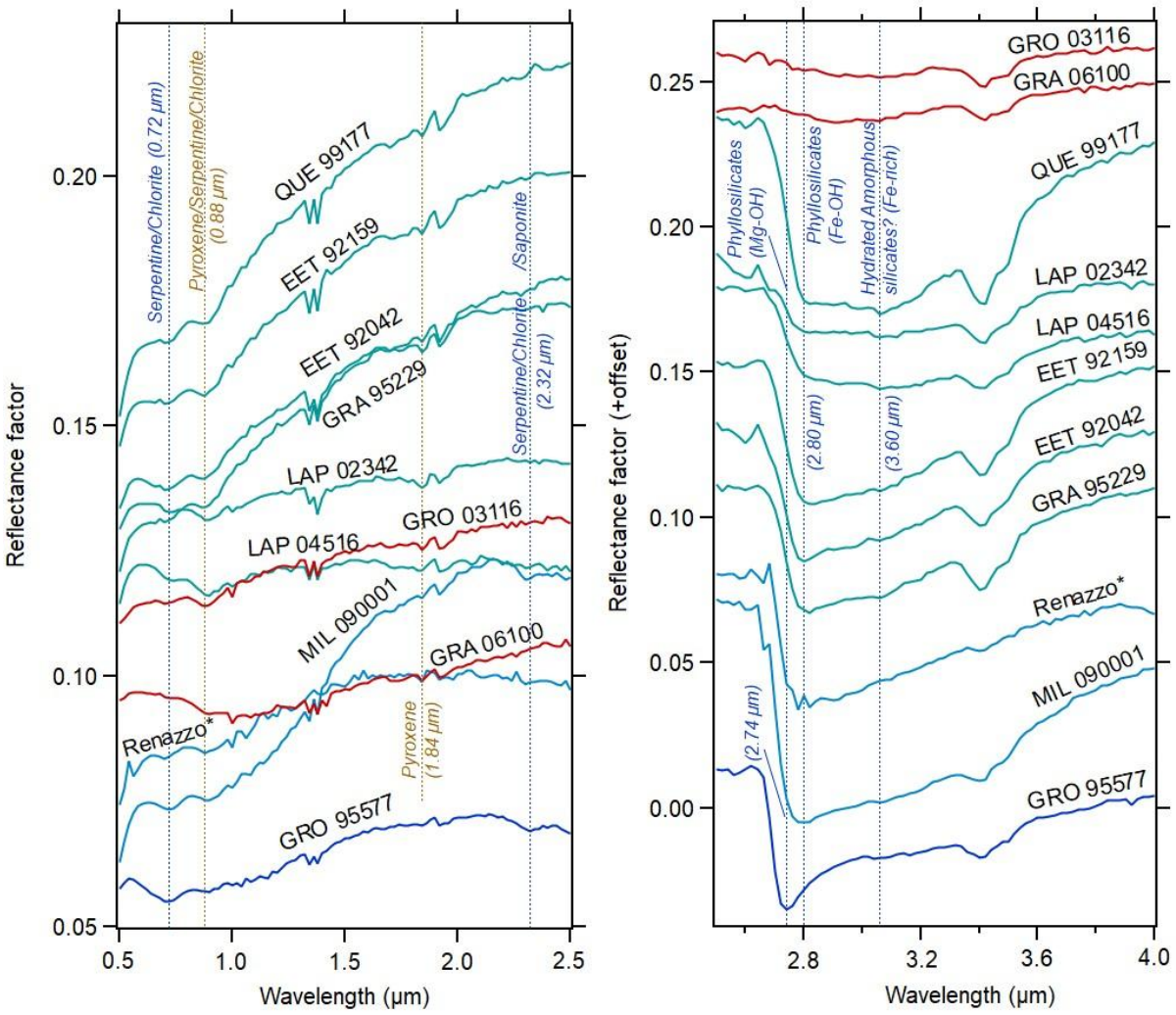

Fig 6. Reflectance spectra of CR chondrites (EATG bulk leached powders), in the VNIR range (left) and around 3-μm (right), plus Renazzo (a CR "fall"). The colors of the spectra correspond to those reported in Fig. 1 and 2. More specifically: Dark Green: enstatite-dominated spectra; turquoise: enstatite-dominated with hints of amorphous or phyllosilicates; light blue: moderately altered CR2s, dominated by phyllosilicates signatures; dark blue: completely hydrated CRs, showing only phyllosilicates in their bulk spectra; red: thermally metamorphosed CRs. Vertical lines have also been added to describe the absorption features present and their associated minerals.

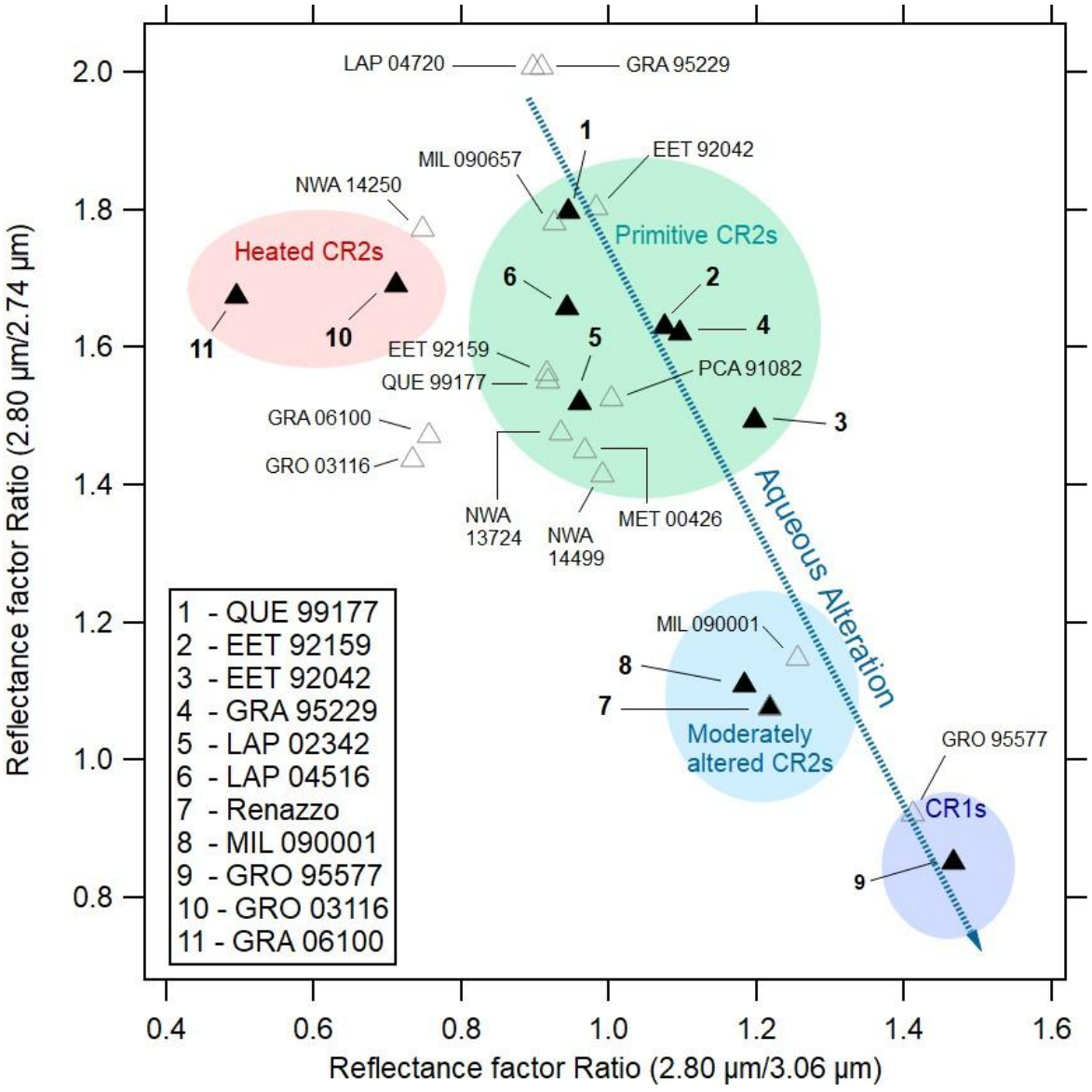

Fig. 7: Spectral parameters from Tables 2 and 3 ("normalized" reflectance factor ratios), containing both leached and untreated data. Based on these values, one can distinguish the 3-µm band profiles of leached CRs into four categories. The diversity is, among other factors, representative of the crystallographic order of hydrated silicates and their Fe-Mg content. Black triangles and gray open triangles correspond to values calculated from spectra of leached and untreated reflectance spectra, respectively.

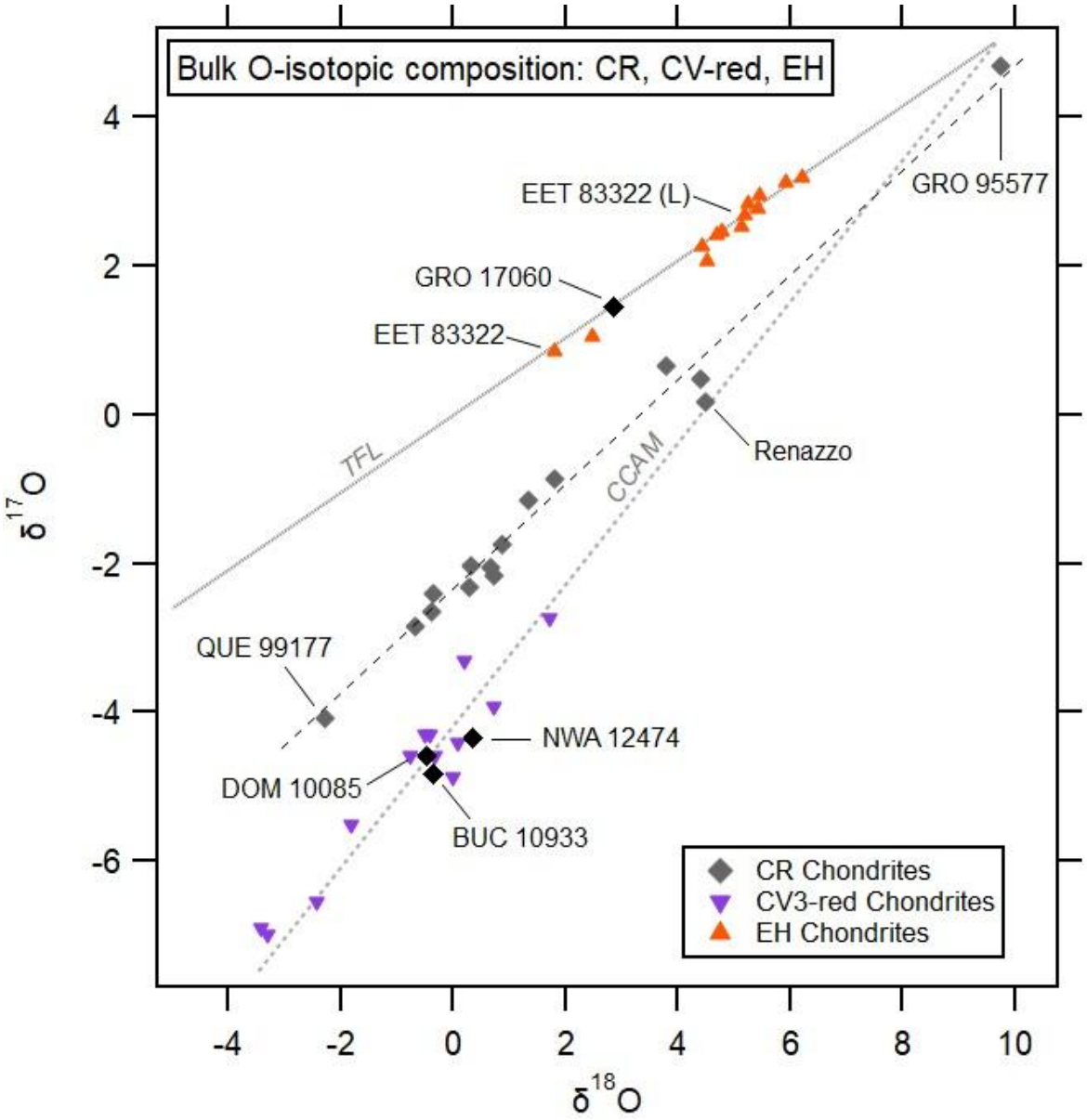

Fig. 8: Bulk oxygen isotopic composition of various CRs (Schrader et al., 2011; Keller et al., 2012; Harju et al., 2014, and this work), CV3-red chondrites (Davidson et al. 2014; Gattacceca et al, 2020 and references therein) and EH3-5s (Clayton et al., 1984, Newton et al., 2000). Note that BUC 10933, DOM 10085, and NWA 12474 (the samples that we measured) fall off from the CR trend, being similar to CV chondrites. GRO 17060 appears to be associated with EH chondrites. "EET 83322 (L)" refers to leached measurements done on this meteorite by Newton et al. (2000).

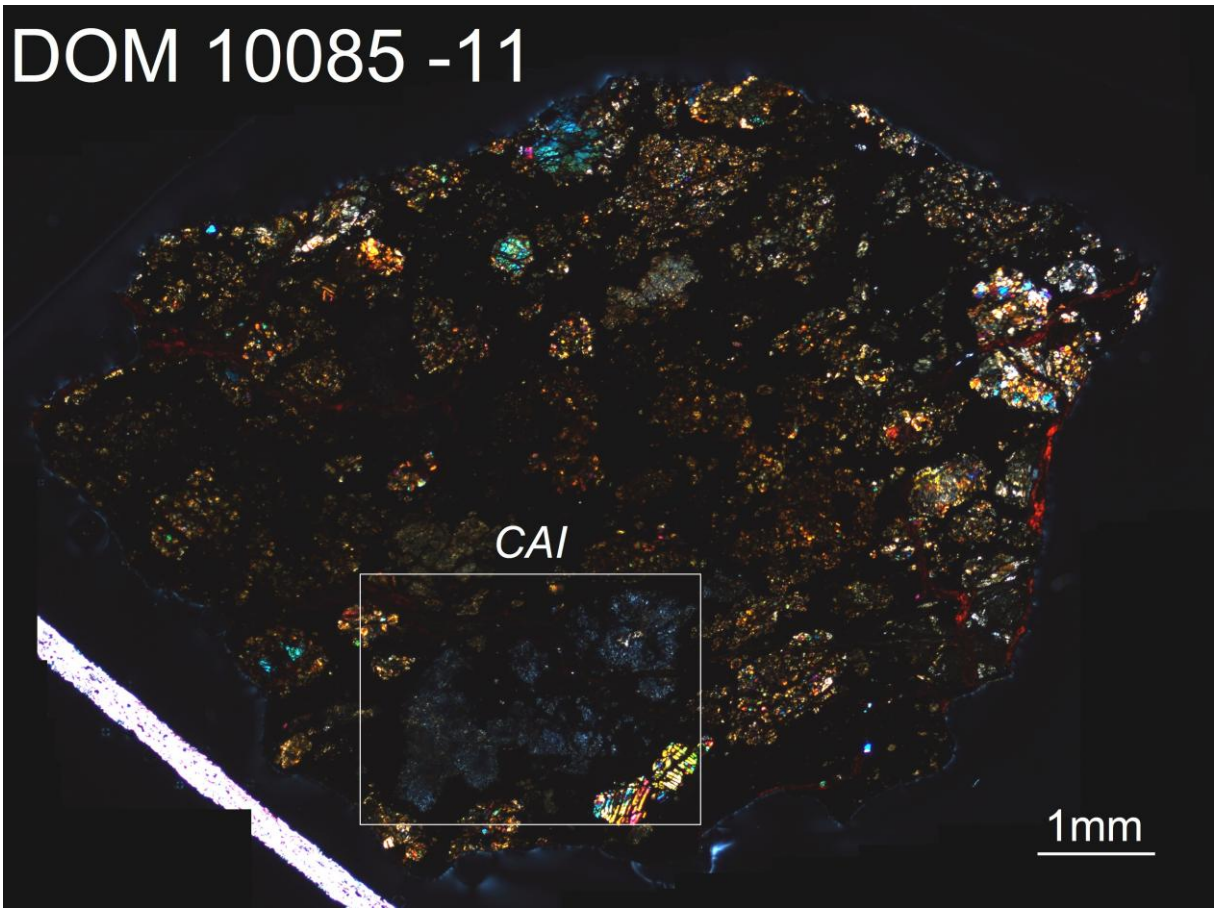

Fig. 9: Mosaic taken under cross-polarized light of the thin section DOM10085-11 at CEREGE. Note the large chondrules, as well as a particularly large (~3 mm) CAI. CAIs, particularly of that size, are typically rare in CRs although common in CV chondrites.

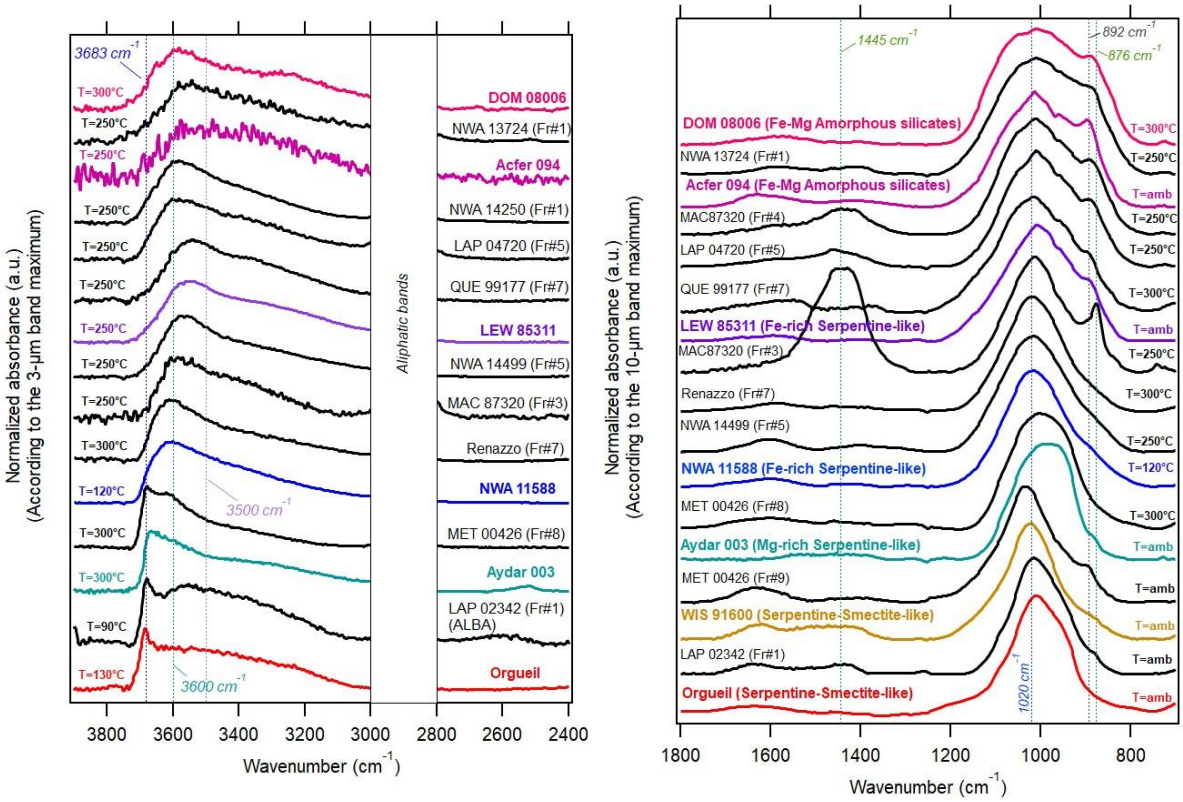

Fig. 10: Comparison between the IR spectra of CR matrix fragments compared to those of other carbonaceous chondrites: DOM 08006 (CO3.0), Acfer 094 (C2-ung), LEW 85311 (CM2-an), NWA 11588 (CM2), Aydar 003 (CM1/2), WIS 91600 (C2-ung) and Orgueil (CI1). We chose to compare these spectra with CRs for the purpose of identifying, more specifically, the mineralogy of the "phyllosilicate-like" phases present in their matrices. The corresponding composition for each of the non-CR chondrites are based on the following literature (see text, section 4.2). The Si-O stretching band of Orgueil and WIS 91600 are likely strongly influenced by smectites (saponite), as they have "sharper" profiles and do not resemble CMs. However, we must note that phyllosilicates in WIS 91600 are deformed, which could affect its spectral properties. Offset has been added for the purpose clarity.

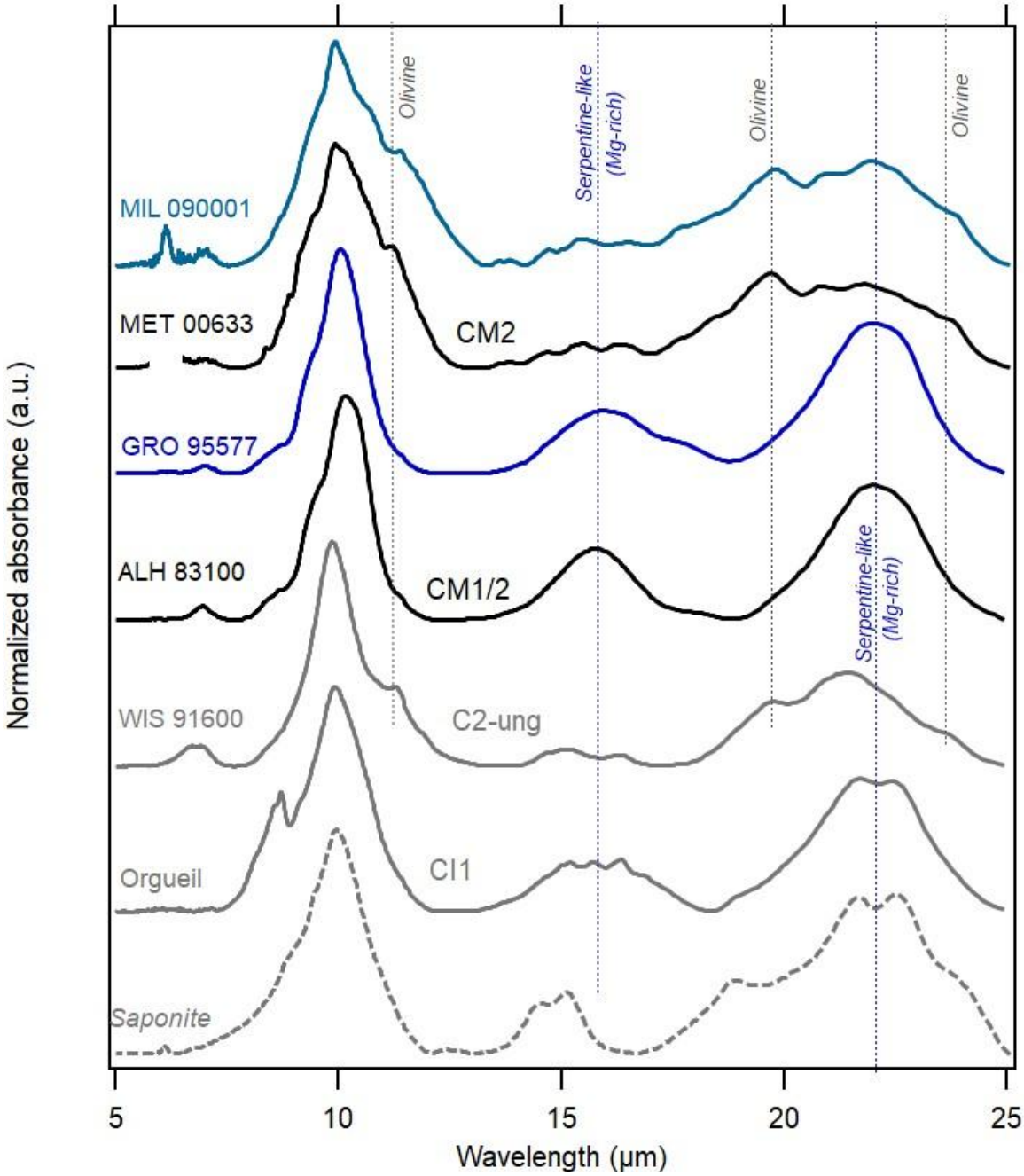

Fig. 11: Bulk MIR spectra of MIL 090001-120 (the one with the strongest phyllosilicate-like signatures) and GRO 95577 (published in Beck et al., 2014), compared to those of a mildly altered CM chondrite (MET 00633) and a CM1/2 chondrite (ALH 83100), Orgueil (CI1), WIS91600 (C2-ung) and terrestrial Mg-rich saponite. The resemblances between these CRs and CMs suggest that MIL 090001 and GRO 95577 are relatively rich (or have a strong spectral contribution) due to serpentine-like minerals. The profiles are different from Orgueil and WIS 91600, suggesting that their bulk serpentine-like content Offset has been added for the purpose of clarity.

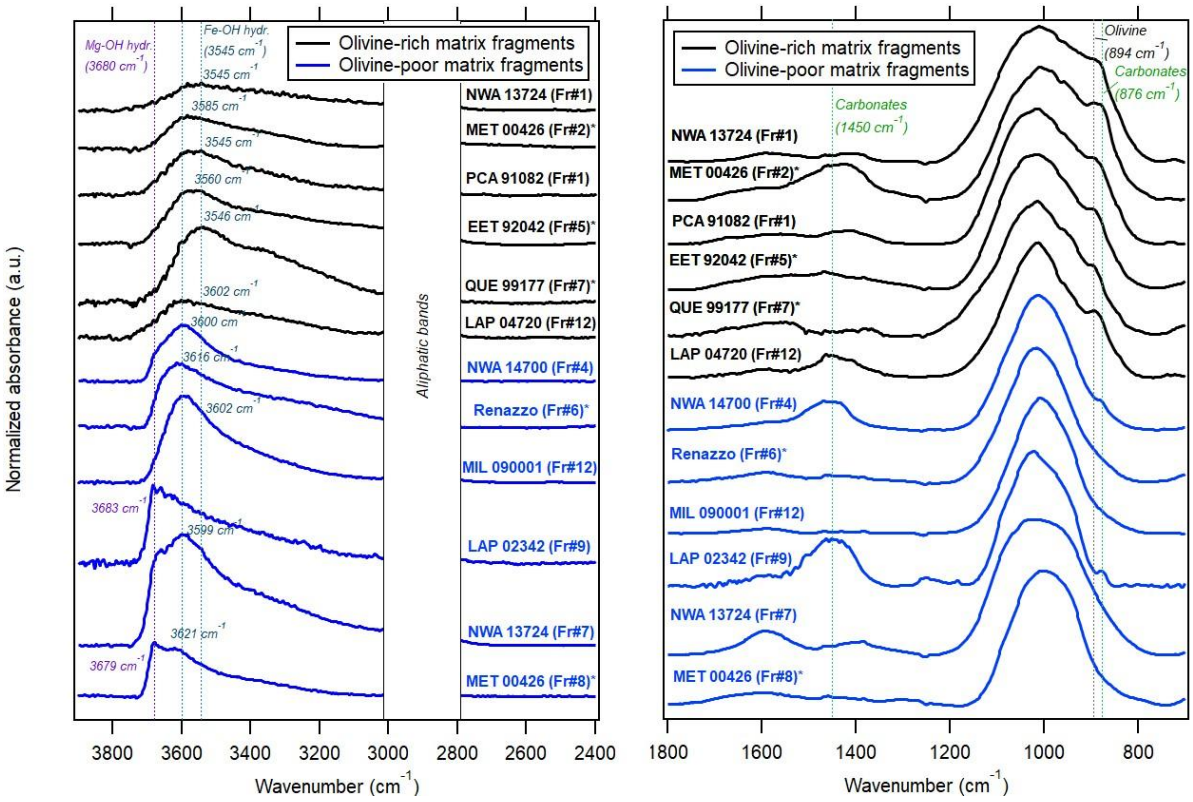

Fig. 12: Comparison between matrix IR spectra rich in olivine (black) compared to IR matrix fragments with no clear detection of olivine signatures (blue). We notice that the 3-µm band tends to peak at lower wavelengths (higher wavenumbers) in the case of olivine-poor fragments. Those richer in olivine tend to also be less asymmetric and "sharp". Purple (3680 cm^{-1} corresponds to Mg-OH bonds in phyllosilicate-like minerals, while the remaining (those at lower wavenumbers) refer to their Fe-OH counterpart. All spectra were taken under 250°C and are normalized according to the 10-µm band peak.

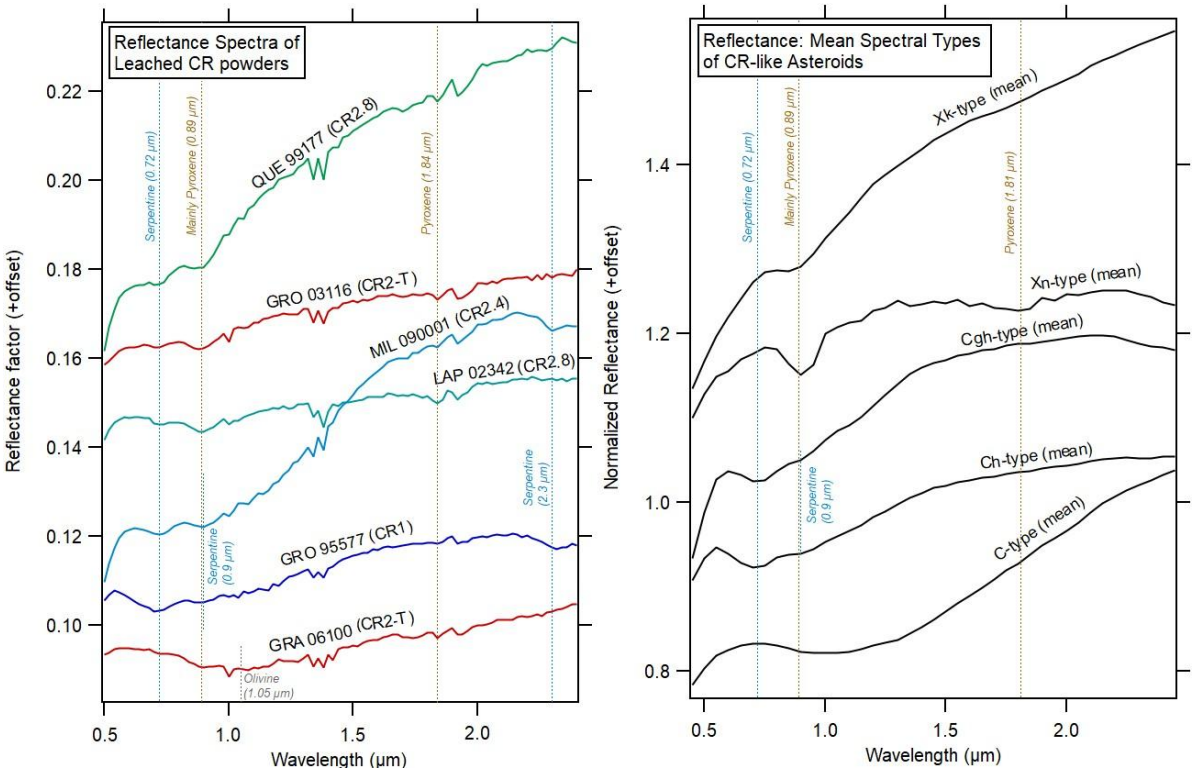

Fig. 13: Comparison between leached CR spectra and mean asteroid spectral types with similar profiles. The figures show that CR chondrites may originate from a diversity of asteroid spectral types, mainly dependent on their secondary history. Even the most primitive of CR2s (e.g. QUE 99177 and LAP 02342) differ from Xk-type asteroids due to the presence of serpentine and/or chlorite signatures at 0.7-µm. The optical drop-off of CRs tend to be at longer wavelengths than X-complex asteroids, perhaps also partially owing to their phyllosilicate content.